Host-rock deformation during the emplacement of the Mourne Mountains granite pluton: Insights from the regional fracture pattern

Tobias Mattsson[1], Steffi Burchardt[1], Karen Mair[2], and Joachim Place[1,*]

[1]Department of Earth Sciences, Uppsala University, Villavägen 16, 752 36, Uppsala, Sweden
[2]Physics of Geological Processes, The NJORD Center, Department of Geosciences, University of Oslo, Box 1047, Blindern, 0316 Oslo, Norway

ABSTRACT

The Mourne Mountains magmatic center in Northern Ireland consists of five successively intruded granites emplaced in the upper crust. The Mourne granite pluton has classically been viewed as a type locality of a magma body emplaced by cauldron subsidence. Cauldron subsidence makes space for magma through the emplacement of ring dikes and floor subsidence. However, the Mourne granites were more recently re-interpreted as laccoliths and bysmaliths. Laccolith intrusions form by inflation and dome their host rock. Here we perform a detailed study of the deformation in the host rock to the Mourne granite pluton in order to test its emplacement mechanism. We use the host-rock fracture pattern as a passive marker and microstructures in the contact-metamorphic aureole to constrain large-scale magma emplacement-related deformation. The dip and azimuth of the fractures are very consistent on the roof of the intrusion and can be separated into four steeply inclined sets dominantly striking SE, S, NE, and E, which rules out pluton-wide doming. In contrast, fracture orientations in the northeastern wall to the granites suggest shear parallel to the contact. Additionally, contact-metamorphic segregations along the northeastern contact are brecciated. Based on the host-rock fracture pattern, the contact aureole deformation, and the north-eastward–inclined granite-granite contacts, we propose that mechanisms involving either asymmetric "trap-door" floor subsidence or laccolith and bysmalith intrusion along an inclined or curved floor accommodated the emplacement of the granites and led to deflection of the northeastern wall of the intrusion.

■ 1. INTRODUCTION

The emplacement of large volumes of granitic magma in Earth's crust is a long-standing problem that has led to much debate since the Earth sciences emerged as a modern scientific discipline (e.g., Cloos, 1922; Read, 1957; Hutton et al., 1990; Pitcher, 1997; Tikoff et al., 1999; Petford et al., 2000;

*Now at Sweco, Gjörwellsgatan 22, 112 60 Stockholm, Sweden

Burchardt, 2018). This so-called "space problem" (e.g., Daly, 1903; Bowen, 1948; Read, 1957; Buddington, 1959) is not only of significance for the question of how the continental crust formed, but is also of importance for understanding hazards related to the emplacement of magma bodies under active volcanoes and the formation of geothermal heat sources and ore deposits (e.g., Richards, 2003; Kennedy et al., 2012; van Wyk de Vries et al., 2014; Kennedy et al., 2018). A better understanding of the mechanisms of granitic magma emplacement can, for example, help decipher the relationship between magma movement in the shallow crust and ground deformation at active volcanoes.

The granites of the Mourne Mountains in the northeastern part of the island of Ireland represent one of the final iterations of the British and Irish Paleogene Igneous Province (Fig. 1A) (Thompson et al., 1987; Gibson et al., 1987, 1995; Gamble et al., 1999; Wilkinson et al., 2017). The Mourne Mountains magmatic center consists of five granites emplaced into Silurian Hawick Group sediments of the Caledonian Southern Uplands–Down-Longford terrane (Anderson, 2000, 2004; Cooper and Johnston, 2004) (Figs. 1 and 2). However, Hood (1981) noted that it is possible to divide the pluton into more units. The study of the Mourne granite pluton by Richey (1927) introduced the idea that pluton formation can be incremental and popularized the magma emplacement mechanism of cauldron subsidence (Fig. 3A). Cauldron subsidence encompasses subsidence of a block of country rock along ring faults within the crust, while magma is transferred along the ring-fault system into the space created above the subsiding block (Clough et al., 1909). Richey (1927) based his interpretation of the emplacement mechanism on the observations that the host rock close to the Mourne granite pluton did not display distinct deformation related to granite emplacement and that the intrusion contacts are mainly discordant to the host-rock bedding (i.e., the granites truncate the bedding). Thus, doming of the roof was viewed as unlikely.

The host rock to the Mourne granites has experienced multi-phase deformation during the Caledonian orogeny (Anderson, 1987, 2000) and is generally not well exposed in the Mourne Mountains. Consequently, there has been some debate about the mechanism of granite emplacement. Several authors pointed out caveats in Richey's (1927) model after remapping the granites and
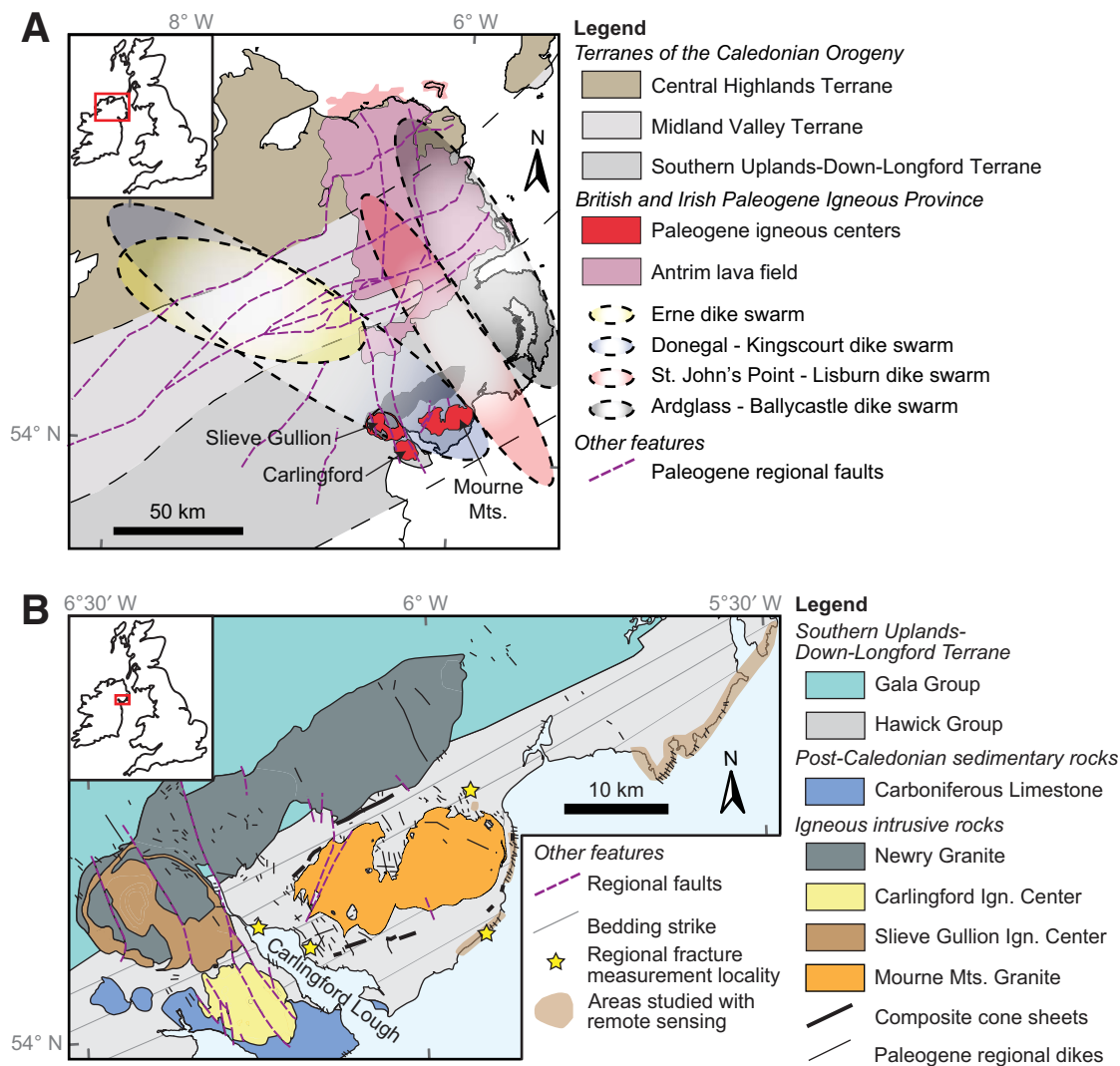
Figure 1. (A) Simplified structural geology map of the northern part of the island of Ireland (based on the 1:100,000 geologic map of Ireland and the 1:650,000 geologic map of the UK with the permission of the British Geological Survey and the Irish Geological Survey). The locations of the Paleogene faults and dikes were based on information from Cooper et al. (2012). The location and orientation of the Paleogene dike swarms are indicated on the map as ellipses. (B) Geological map of the eastern coast of the island of Ireland (based on Anderson, 2004; Cooper and Johnston, 2004; and the 1:100,000 geologic map of Ireland and the 1:650,000 geologic map of the UK with the permission of the British Geological Survey and the Irish Geological Survey). The thin gray lines show the general strike of the bedding in the Hawick Group. Composite cone sheets surrounding the Mourne granite pluton are shown on the map as thick black lines (the locations of the sheets were based on maps by Tomkeieff and Marshall, 1935; Emeleus, 1955; Emeleus and Preston, 1969; Akiman, 1971), while regional dikes are shown as thin black lines (based on maps from Traill, 1871; Tomkeieff and Marshall, 1935; Akiman, 1971). Yellow stars indicate fracture-study localities located farther than two kilometers from the granite pluton. Areas studied with remote sensing are highlighted with brown polygons. The maps contain Irish Public Sector Data (Geological Survey) licensed under a Creative Commons Attribution 4.0 International (CC BY 4.0) license and public sector information licensed under the Open Government License v. 3.0.

the contacts to and within the intrusion, which led to refinements of the cauldron subsidence emplacement model for the Mourne granite pluton (Emeleus, 1955; Robbie, 1955; Hood, 1981; Gibson, 1984; Meighan et al., 1984). However, other models for the emplacement of the Mourne granites have also been presented. Rohleder (1931), for example, interpreted the granites as discordant laccoliths. Laccolith intrusions form in the shallow crust by deforming

and uplifting their host rock (Gilbert, 1877; Johnson and Pollard, 1973). Walker (1975) proposed that the Mourne granites were fed laterally from a source in the NE into space created by an internally sagging dense mafic body. This process evokes subsidence of the underlying material, but not along ring faults. Two more recent anisotropy of magnetic susceptibility (AMS) studies on the Mourne granite intrusions by Stevenson et al. (2007) and Stevenson
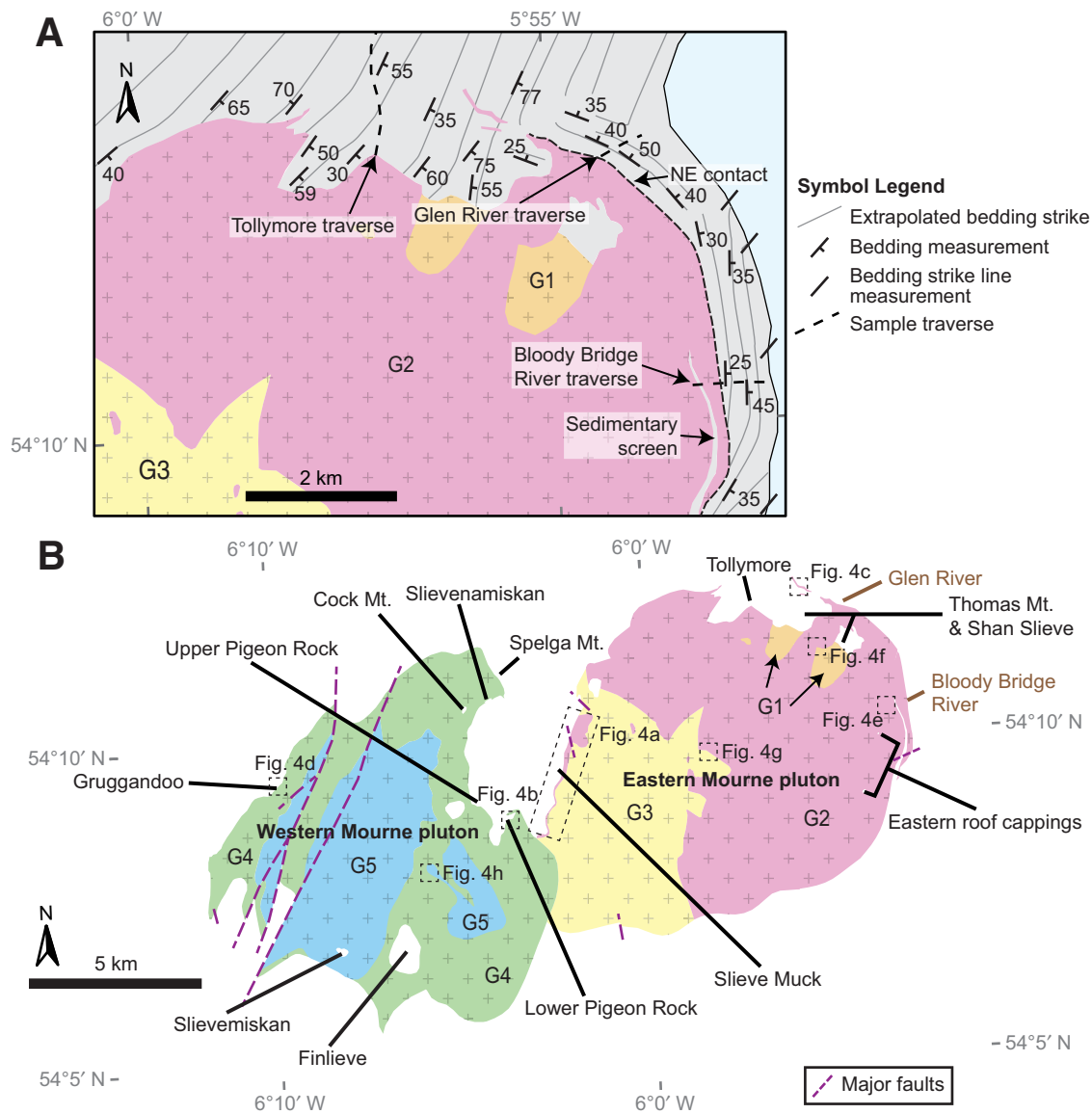
Figure 2. (A) Map of the northern and the northeastern contact of the Eastern Mourne pluton (redrawn after Hood, 1981). Bedding measurements and extrapolated and interpreted bedding strike next to the northeastern contact to the Mourne granite pluton are shown on the map (data from Traill, 1871; Hood, 1981; this study). Dashed black lines indicate the sample traverses through the contact-metamorphic aureole. (B) Geological map of the five granites (G1 to G5) that constitute the Mourne granite pluton (redrawn after Hood, 1981 and Gibson, 1984). G1 is the oldest granite, and G5 is the youngest. The fracture-study localities and locations of photographs in Figure 4 are indicated on the map. Wall outcrops are shown by dark-brown text and roof outcrops by black text. See main text for the definition of a wall and roof outcrop.
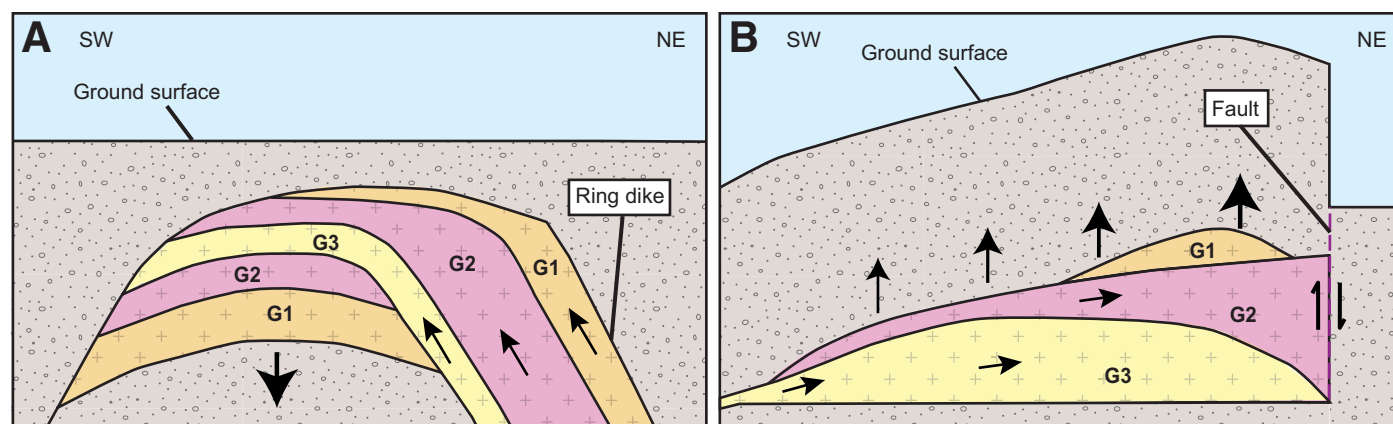
Figure 3. Sketch of previously published models of the emplacement of the Eastern Mourne granite pluton (G1–G3). (A) Cauldron subsidence model of Richey (1927). Figure modified after Richey (1927). (B) Partly faulted laccolith and bysmalith emplacement model of Stevenson et al. (2007), which implies that part of the host rock is uplifted along a fault. The smaller black arrows indicate magma flow and the larger black arrows indicate the displacement of the host rock. The sketches are vertically exaggerated.

and Bennett (2011) interpreted that the granites of the eastern part of the pluton were emplaced both as laccoliths and bysmaliths, while the granites intruded as laccoliths in the western part of the pluton (Fig. 3B). They based their interpretation on a subhorizontal magnetic fabric in the center of the intrusion, magnetic fabrics with shallow dips at the contacts in the eastern part of the pluton, the divergent strikes of the Southern Uplands–Down-Longford terrane bedding along the granite pluton's northeastern boundary (Fig. 2A) (Hood, 1981), and remapping of granites (Meighan et al., 1984).

Because of the preexisting deformation from the Caledonian orogeny (e.g., Anderson, 1987, 2000) and sparse exposures, the deformation of the host rock associated with the emplacement of the Mourne granite pluton remains poorly understood. In this study, we investigate the emplacement mechanism of the Mourne granite pluton using fractures in the granites and the fracture patterns in the host rock as proxies for deformation. Our approach includes fracture data rotation analysis based on the dip and strike of the contact to shed more light on granite emplacement from the perspective of host-rock deformation. We also provide observations on the contact aureole to the Mourne granite pluton in order to constrain the timing of deformation relative to granite emplacement. By combining previous research on the Mourne granite pluton with our new data, we discuss models for the emplacement of the granites.

Our analyses reveal that the intrusion roof does not display pluton-wide doming, while the northeastern wall of the intrusion records significant deformation, which suggests shear parallel to the strike of the contact. We propose that the Mourne granite pluton was emplaced by asymmetric floor subsidence or laccolith intrusion along a curved floor, which could explain the lack of doming of the roof.

1.1. Laccoliths

Laccolith intrusion involves making space for magma by pushing upwards and deforming the host and the magma body (e.g., Gilbert, 1877; Hawkes and Hawkes, 1933; Pollard and Johnson, 1973; Hutton, 1988). Laccolith growth can be divided into three stages: (1) Magma intrudes and forms a sill, followed by (2) inflation of the sill to form a laccolith, and finally (3) the bysmalith stage where the host rock is uplifted along faults (de Saint-Blanquat et al., 2006). The growth of the magma body may terminate at any of the above-mentioned stages yielding different types of magmatic intrusions (namely sills, laccoliths, and bysmaliths). Deformation of the host rock associated with laccolith growth involves rotation and uplift, faulting, and minor bending (de Saint-Blanquat et al., 2006; Morgan et al., 2008; van Wyk de Vries et al., 2014; Wilson et al., 2016; Mattsson et al., 2018). In case of the inflated-sill laccolith type, the host rock should largely drape the dome-shaped laccolith (Gilbert, 1877; Hawkes and Hawkes, 1933). In contrast, the host rock to stacked sill- and bysmalith-type laccoliths should overall retain its original inclination except at the edges of the laccolith where it should be rotated and bent and/or faulted (Corry, 1988; de Saint-Blanquat et al., 2006; Morgan et al., 2008; Wilson et al., 2016). Even if a laccolith has a flat roof and the host was uplifted in a piston-like fashion, some discernible deformation should occur at the flanks of the intrusion.

1.2. Cauldron Subsidence

Cauldron subsidence was first described by Clough et al. (1909) for Glen Coe, Scotland, and is a type of subterranean caldera collapse (Richey, 1927;

Paterson and Fowler, 1993; Cruden and McCaffrey, 2001; Yoshinobu et al., 2003; Burchardt et al., 2012). Cauldron subsidence can be grouped into magma emplacement mechanisms that involve floor subsidence (e.g., Cruden, 1998; Cruden and McCaffrey, 2001). Here, cauldron subsidence is distinguished as floor subsidence facilitated by faults that are related to magmatic activity such as outward inclined ring faults with a bell-jar geometry (cf. Anderson, 1937), as opposed to floor subsidence that is controlled by regional faults (e.g., Holohan et al., 2005). The mechanisms causing cauldron subsidence have been likened with caldera collapse, in which removal of magma from an underlying reservoir induces subsidence at Earth's surface (e.g., Cruden, 1998; Cruden and McCaffrey, 2001; Branney and Acocella, 2015).

■ 2. GEOLOGICAL SETTING

The following section summarizes (1) the deformation of the Hawick Group that occurred during the Caledonian orogeny and in the Paleogene and (2) previous research on the Mourne granite pluton.

2.1. Southern Uplands–Down-Longford Terrane

The Southern Uplands–Down-Longford terrane trends ENE-WSW through southern Scotland, Northern Ireland, and Ireland and is made up of a succession of isoclinally folded turbidite tracts or blocks bounded by major thrust faults (Anderson and Cameron, 1979; Anderson, 2000). The terrane youngs toward the SE and has been interpreted as a relict accretionary prism that formed during the Caledonian orogeny (Anderson, 2004). The Hawick Group is situated at the front of that accretionary prism and consists of a fine-grained graywacke with interbedded sandstone, siltstone, and dark shale layers (Anderson, 2004). The graywacke consists of quartz, chlorite, epidote, minor amounts of iron oxides, sericite, and altered feldspars (Emeleus, 1955). Carbonates are also abundant in the groundmass, as well as in concretions and nodules in Hawick Group rocks (up to 20 vol%, Emeleus, 1955; Anderson, 2004).

The axial surface of isoclinal folds in the Hawick Group strikes 067°, which is parallel to the dominant strike of the bedding (Fig. 1A) (Anderson, 1987). North of the Mourne Mountains, the dominant strike of the Hawick Group (and the Southern Uplands–Down-Longford terrane) bedding changes to ~037° (Beamish et al., 2010). However, no distinct change to bedding strikes within the Hawick Group has been reported in the vicinity of the Mourne Mountains (Hood, 1981; Gibson, 1984). Structures related to three phases of deformation (D_1 to D_3) have been mapped in the Southern Uplands–Down-Longford terrane. D_1 (cleavage) developed parallel to the axial plane of the isoclinal folds (and the fault-bounded blocks). The fold axis of F_1 folds is generally shallowly plunging (Anderson, 1987, 2000). D_2 created a crenulation on the D_1 cleavage that verges to the south, and D_3 generated steeply plunging folds (Anderson, 2000). The D_1 to D_3 deformation has been interpreted to be caused by regional sinistral trans-

pression (Anderson, 1987, 2000). Brittle deformation occurred during the waning stages of the Caledonian orogeny (Anderson, 2000). Two sets of sinistral strike-slip faults and a set of dextral strike-slip faults displace the Hawick Group and record dominant strikes of 195°, 355°, and 125°, respectively (Anderson, 1987). The slip on these faults ranges from a few centimeters to 100 m. The regional metamorphic grade of the Southern Uplands–Down-Longford terrane varies between zeolite and prehnite-pumpellyite facies caused by burial during accretion down to 12 km depth (Oliver and Leggett, 1980; Merriman and Roberts, 2001).

2.2. Paleogene Tectonics

During the early Paleogene, the principal tectonic stresses affecting the Southern Uplands–Down-Longford terrane of Northern Ireland were caused by the far-field Alpine orogeny that created two large strike-slip conjugate fault sets that trend NNW-SSE and ENE-WSW (Fig. 1A) (Cooper et al., 2012). At the onset of the opening of the North Atlantic during the formation of the British and Irish Paleogene Igneous Province, mantle plume–related tectonics became dominant (Lawver and Muller, 1994; Emeleus and Bell, 2005). Four major dike swarms display the stress field of plume-related rifting (Fig. 1A). The two oldest dike swarms, (1) the Erne dike swarm that strikes primarily WNW-ESE and (2) the Donegal–Kingscourt dike swarm that strikes NW-SE, are overlain by the Antrim lavas and therefore intruded before ca. 62 Ma (Cooper, 2004; Ganerød et al., 2010; Cooper et al., 2012). (3) The Ardglass-Ballycastle dike swarm that strikes from NNW-SSE to WNW-ESE has a bracketed age between ca. 62 and 59 Ma (Cooper, 2004; Ganerød et al., 2010; Cooper et al., 2012). The youngest dike swarm, (4) the St. John's Point–Lisburn dike swarm, consists of NNW-SSE–striking dikes that intrude the Antrim lavas but are truncated by the Mourne granite pluton. This suggests an age of the St. John's Point–Lisburn dike swarm between ca. 59 and 56 Ma (Cooper, 2004; Cooper and Johnston, 2004; Ganerød et al., 2010; Cooper et al., 2012; see also section below). The stress fields of the igneous centers in northeastern Ireland have locally affected the trend of the dike swarms (Cooper et al., 2012). There is evidence of reactivation of the Paleogene faults in Northern Ireland after the end of magmatic activity, but no major tectonic event occurred in the area of the Mourne Mountains after the emplacement of the granites (Johnston, 2004; Quinn, 2006; Cooper et al., 2012).

2.3. The Mourne Mountains Magmatic Center

The Mourne granite pluton is exposed in a mountainous area along the southeastern coast of Northern Ireland (Fig. 1). The granite pluton has been treated as two separate magmatic centers, an eastern and western center (Fig. 2A) (Emeleus, 1955; Hood, 1981; Gibson, 1984; Meighan et al., 1984; Cooper and Johnston, 2004; Stevenson et al., 2007; Stevenson and Bennett, 2011). However,

mapping has shown that the granites form a connected pluton (Richey, 1927; Emeleus, 1955; Hood, 1981; Gibson, 1984). The oldest granites, G1 to G3, form the eastern part of the pluton, and the younger granites, G4 and G5, form the western part (Fig. 2B) (Cooper and Johnston, 2004). Radiometric ages of granites G1 to G4 overlap within the error of the applied methods, suggesting that the bulk of the pluton was assembled rapidly at ca. 56 Ma (cf. Gibson et al., 1987, 1995; Gamble et al., 1999; Wilkinson et al., 2017), while G5 yields a slightly younger age of 54.6 ± 1.0 Ma ($^{40}Ar/^{39}Ar$, Gibson et al., 1995). In the eastern Mourne Mountains, the granites are exposed at higher elevations (up to 850 m) than the western Mourne Mountains (up to 638 m), which can be interpreted, together with estimates of contact location and dip, as due to ~200 m or more difference in intrusion depth (cf. Gibson, 1984). Allen et al. (2002) estimated that ~3000 m of overlying rock have been eroded from the Mourne granites since their emplacement.

The Mourne dike swarm is mafic in composition and located to the east and SE of the Mourne granite pluton (Akiman, 1971). The Mourne dike swam displays strike orientations (NW-SE and NNW-SSE) similar to the regional Donegal and Kingscourt and St. John's point and Lisburn dike swarm (Tomkeieff and Marshall, 1935; Cooper et al., 2012) and might therefore be an extension of these two swarms (Fig. 1). The Mourne granite pluton is only sparsely intruded by dikes and interpreted to be younger than the dike swarms (Akiman, 1971; Hood, 1981; Cooper et al., 2012). Additionally, several moderately inclined magmatic sheets that dip toward the Mourne granite pluton are exposed in the surrounding graywacke. These magmatic sheets are mafic to felsic in composition and commonly composite. Composite sheet exposures occur at localities surrounding the eastern and western part of the Mourne Mountains (Fig. 1B). The sheets are generally inclined at an angle of ~35° toward the granite pluton and might therefore be a circumferential exposure of the same (cone) sheet that originated from beneath the current exposure of the Mourne granite pluton (cf. Richey et al., 1930; Anderson, 1937; Akiman, 1971; Burchardt et al., 2013). The granites in the western part of the Mourne Mountains truncate the composite sheet. The "Mourne" dike swarm is cut by a composite magmatic sheet at the mouth of the Bloody Bridge River and is therefore interpreted to be older than the observed composite sheets close to the Mourne granite pluton (Emeleus, 1955; Akiman, 1971).

The graywacke next to the Mourne granites has been altered to hornfels (Richey, 1927; Emeleus, 1955). Emeleus (1955) distinguished two different types of hornfels: one type consisting of quartz, plagioclase, and oxides, the second type is banded with biotite (blue bands) and diopside (green bands), where Emeleus (1955) interpreted the banding as a relict sedimentary feature.

In the northeastern part of the Eastern Mourne pluton, the contact with the Silurian graywacke dips moderately outward from the center of the pluton (35–~50° NE) and has been suggested to represent the wall (or a lateral contact) of the granite pluton (Richey, 1927; Hood, 1981). This contact is terminated at both ends by granitic dike-like tips parallel to the contact (Figs. 2A and 4C). Richey (1927) therefore interpreted the northeastern contact to the Eastern Mourne pluton to represent part of the feeding ring dike to the granite pluton.

Stevenson et al. (2007) and Stevenson and Bennett (2011) analyzed magnetic (AMS) fabrics in the Mourne Mountains granites. The magnetic fabric in the Mourne granite pluton is dominantly oblate to triaxial. In G1 and the bulk of G2, the magnetic fabric dips outward from the center of the pluton. The dip of the magnetic fabric is moderate to steep in G1 and shallow in G2. In the southwestern part of the Eastern Mourne pluton, on the other hand, the fabric is largely triaxial to oblate, subhorizontal, and no dominant dip direction can be observed. In G3, the fabric is dominantly triaxial to weakly oblate with a subhorizontal foliation and lineation. In some parts of G3, the foliation is subvertical and strikes NE-SW. Stevenson et al. (2007) interpreted the generally subhorizontal fabric in the interior of the Eastern Mourne pluton and contact parallel fabric in the eastern and northeastern part of the pluton as evidence that the granites were fed laterally either from the NE or SW. They further interpreted the northeastern contact as a fault, attributing its formation to roof uplift during bysmalith inflation (Figs. 2A and 3B). In the central and southern part of the Western Mourne pluton, the magnetic fabric is subhorizontal, and the magnetic lineation trends NNE-SSW. In the western, northeastern, and eastern parts of the Western Mourne pluton, the magnetic fabric dips shallowly outward from the center of the pluton. Some of the magnetic lineations in the eastern part of the pluton are subhorizontal and trend N-S. Based on the subhorizontal NNE-SSW trends, magnetic lineation, and contact parallel magnetic foliation in the Western Mourne pluton, Stevenson and Bennett (2011) favored an emplacement scenario where all the Mourne granites were fed from the SW. A large gravity anomaly beneath the Carlingford Lough, SW of the Mourne Mountains, is inferred to represent the mafic source magma chamber to the Mourne granite pluton and to the Slieve Gullion and Carlingford igneous centers (Fig. 1) (Reay, 2004; Stevenson et al., 2007; Stevenson and Bennett, 2011). Notably, the Mourne Mountains are characterized by the absence of a negative gravity anomaly (Reay, 2004).

2.3.1. Contact Relationships in the Eastern Mourne Pluton

Apart from the moderately inclined northeastern contact, all other exposed contacts to the Eastern Mourne pluton in general dip shallowly (10°–30°) away from the center of the granite body, and because the host rock overlies the granite at these localities, they are thought to represent roof contacts (Hood, 1981). The exposed contacts to the Eastern Mourne pluton are always discordant to the bedding of the graywacke (Richey, 1927; Hood, 1981). Fine-grained chill zones occur in the granites, both at the external (granite-graywacke) and internal (granite-granite) contacts (Richey, 1927; Gibson, 1984).

G1 is the least voluminous, the oldest, and geochemically most primitive of the Mourne granites and crops out only on the highest peaks in the northeastern part of the Mourne Mountains (Meighan et al., 1984) (Figs. 2A and 4F). G1 has therefore been assumed to be a relatively thin granite sheet, although its roof is not exposed (Hood, 1981; Meighan et al., 1984). G2 underlies G1,
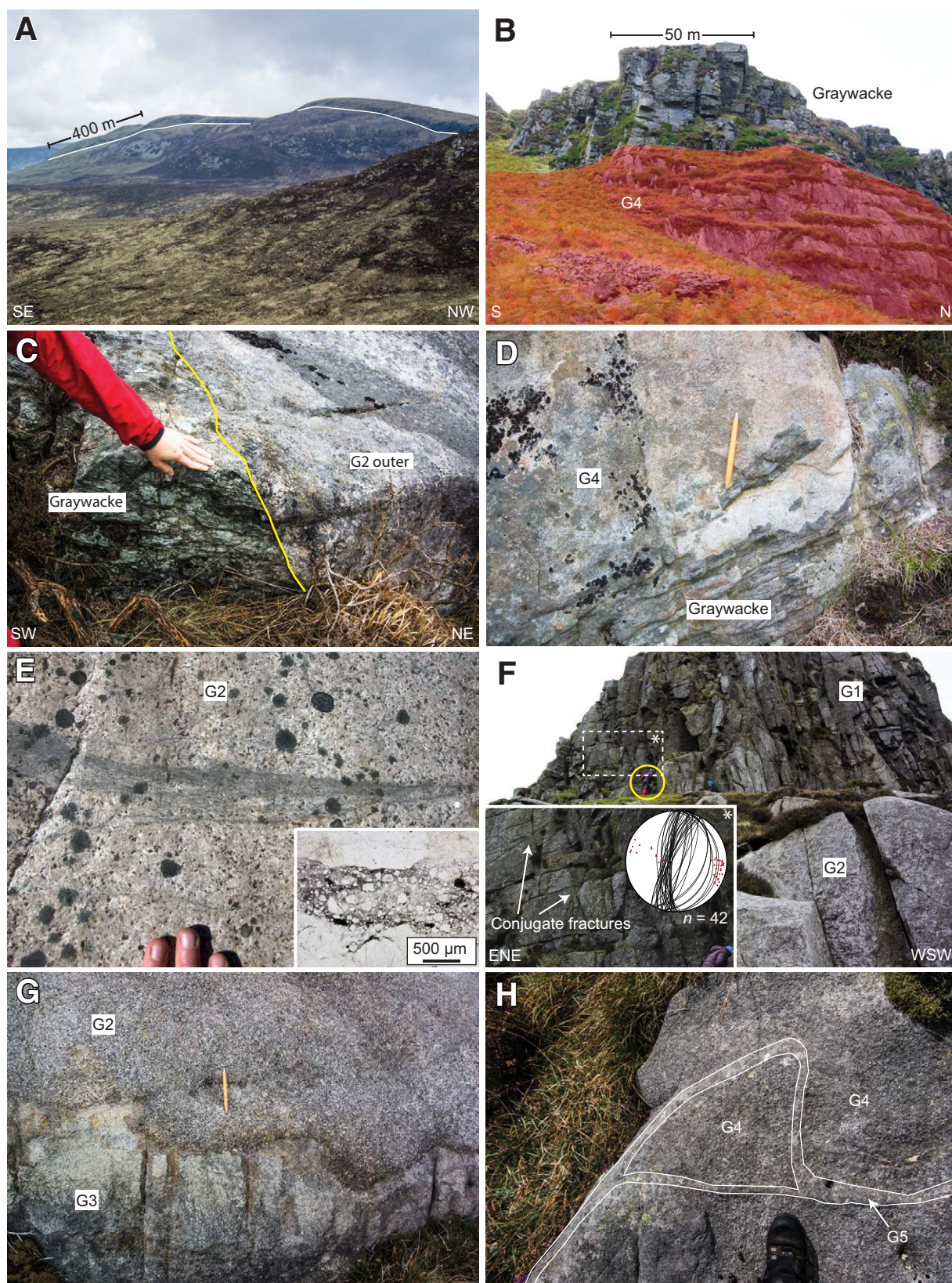
Figure 4. (A) View toward Slieve Muck. The white line indicates the graywacke-granite roof contact. (B) The granite-graywacke roof contact at Lower Pigeon rock. The granites are highlighted in red. Note the fractures in the overlying graywacke, marked by steeply inclined fracture surfaces create distinct relief on the outcrop. (C) Contact between graywacke and the Tullybrannigan River granitic dike that dips to the NNE. The bedding in the graywacke (left hand side of the image) is subhorizontal and discordant to the contact. A thin yellow line marks the contact. (D) Graywacke xenolith (dark rock) in granite G4 (light-colored rock) at Gruggandoo. Orange pen for scale. (E) Dark cataclasite bands in granite G2 located west of the sedimentary screen in the eastern part of the Eastern Mourne pluton. The inset shows a PPL (plane-polarized light) microphotograph of cataclasite in G2 next to the sedimentary screen. (F) Contact between granites G1 and G2 at the northern slopes of Slieve Donard. The overlying G1 is darker and more densely jointed than the underlying G2. Encircled person for scale. Inset shows close-up of conjugate fractures in G1, as well as a lower-hemisphere Schmidt stereonet with orientations of conjugate fractures (planes and poles). (G) Contact between coarse-grained G2 and underlying chilled and fine-grained G3 on the south-southwestern slope of Slieve Lamangan. Orange pen for scale. (H) Exposure of G4 just above the contact to the underlying G5, next to Aughnaleck River. G4 is coarse grained and intruded by fine-grained G5 aplite dikelets. The white lines indicate the contact between the two granites. Boot for scale. The locations of the photographs are given in Figure 2B.

and the contact between the two granites dips ~30° toward NE (Fig. 5). Stevenson et al. (2007) argued that the inclination of the G1-G2 contact is an evidence for up-doming (i.e., laccolith inflation). G2 is composed of a finer- and a coarser-grained variety named G2 outer and G2 inner, respectively. The orientation of the G2 inner-G2 outer contact varies within the granite pluton. In the northwestern and southeastern part of the Eastern Mourne pluton, the contact dips shallowly outward (~20°), whereas in the east, the contact dips moderately outward from the center of the pluton (Fig. 5 and Supplemental Fig. S1[1]) (~50°, Hood, 1981). G3 underlies and is finer grained than G2 (Fig. 4G). The contact between G2 and G3 is clearly exposed on crags and cliffs in the central part of the eastern Mourne Mountains surrounding the Ben Crom reservoir and dips shallowly (<10°) to the NE (Hood, 1981). The contact is in places wavy, but sharp, suggesting that the not-yet-solid G2 crystal mush was eroded by the intruding G3 magma. G3 displays a fine-grained chilled zone at the contact, while G2 is coarse grained (Fig. 4G). Richey (1927) argued that G2 should display a chill zone as well, if G3 intruded along the G2-graywacke floor interface and therefore interpreted that G3 split G2 and that the bottom of G2 subsided as G3 intruded. Close to the G2-G3 contact, centimeter to decimeter in diameter patches of coarser granite (interpreted as older granites of G3 composition or alternatively xenoliths of G2) occur, as well as pegmatite veins, separated leucocratic bands, and mica bands (Hood, 1981). Hood (1981) inferred that the floor to the granites was gently inclined toward the east caused by asymmetric floor subsidence during the emplacement of the granites (see also Cooper and Johnston, 2004). Stevenson et al. (2007) also considered the possibility of a curved floor that dips to the NE in one of their proposed emplacement models for the Eastern Mourne pluton.

2.3.2. Contact Relationships in the Western Mourne Pluton

The graywacke-granite contact in the Western Mourne pluton is generally discordant to the host-rock bedding (Emeleus, 1955; Gibson, 1984). The only location where the contact is concordant to the graywacke bedding is on Slievenamiskan, in the northern part of the Western Mourne pluton (Gibson, 1984). There, the granite-graywacke contact dips between ~20°–35° toward the SE. The chill zone next to the graywacke-granite contact is thinner (~5 mm) where abundant granite dikes have intruded the graywacke, while it is several meters thick where granitic dikes occurs sparsely in the host rock (Gibson, 1984). Pegmatites and drusy cavities are particularly common directly adjacent to the internal (granite-granite) and external (granite-graywacke) contacts. The G4 granite body is dome-like in shape and exposed at the rim of the Western Mourne pluton and at elevations above 310 m above sea level (asl) in the central part of the Western Mourne pluton (Figs. 5 and S1 [footnote 1]) (Gibson, 1984). Outcrop relationships in the area between the Eastern and Western Mourne plutons indicate that G4 truncates G3 and is therefore younger (see also Fig. 5) (Gibson, 1984). G4 is geochemically very similar to granites G2 and G3, but with a distinct texture (Hood, 1981; Gibson, 1984). G5 crops out

below G4 in the central parts of the Western Mourne pluton, and the internal contact between G4 and G5 dips shallowly outward (~10°) from the center of the intrusion (Figs. 5 and S1 [footnote 1]). Xenoliths of G4 (several decimeters in diameter) occur adjacent to the granite-granite contact in G5 in some places, and G5 aplites intrude the G4 joint system (Fig. 4H) (Gibson, 1984). Younger regional faults downthrow the western parts of the Western Mourne granite pluton in several grabens (Fig. 5) (Emeleus, 1955).

■ 3. METHODS

3.1. Field Campaign

Structural orientation data were collected on fractures, contacts, bedding and joints during three field campaigns in April 2015, May 2016, and September 2016 using the FieldMove clino Pro application (www.mve.com/digital-mapping/) with an Iphone 6® in the coordinate system UTM Zone 29N and analogue compasses. The smartphone measurements were regularly double-checked with an analogue compass. The Fieldmove clino pro application corrected the smartphone measurements for the magnetic declination in the field, while the orientation measurements with an analogue compass were corrected for the local magnetic declination (~3.3°W) after the fieldwork. The smartphone compass together with the Fieldmove clino pro application are generally accurate to ±10° (Scott et al., 2016; Allmendinger et al., 2017), and that the error is overcome by the larger amount of data that can be collected compared with an analogue compass (www.mve.com/digital-mapping/). Measurements were collected at localities close to the contact between the graywacke and the granites. Due to sporadic and often small outcrop exposures, systematic line, circle or square fracture mapping was not practical at most localities. We therefore aimed to measure all fractures (i.e., where strike and dip were attainable) over a smaller area (~25 × 25 m) to avoid sampling bias. We did not apply any weighting due to exposure biases for in situ measured fractures. However, certain fracture sets had naturally more relief and might therefore have been favored due to visibility and the orientation of the outcrop surface(s).

To complement the data measured in the field, fractures and bedding in the Hawick Group were measured by marking natural lineaments on outcrops on satellite images along the southeastern coast of Northern Ireland (GLOBALearth) in ESRI ArcGIS™ (https://www.esri.com/en-us/arcgis/). The lineament orientations were analyzed in MOVE 2017.2™ (https://www.mve.com/).

Contact aureole samples were collected during the 2015 field campaign in traverses from the contact up to 1.7 km from the granite in the wall to the Eastern Mourne pluton to constrain the timing of deformation compared to contact alteration. Representative samples were selected for thin section preparation (see Supplemental Table S1 [footnote 1]). Several of the thin sections were analyzed with electron dispersive spectroscopy (EDS) using the field emission source JEOL JXA-8530F Hyperprobe at Uppsala University, Sweden, to identify mineral phases.

───────

[1]Supplemental Materials. Text file describing supplemental material (includes five figures). Table S1 and S4 and virtual scan line data. Table S2 provides all structural data (fractures, contacts, bedding, joints, and lineaments) collected during study. Table S3 provides all scan line data. Please visit **https://doi.org/10.1130/GES02148.S1** or access the full-text article on www.gsapubs.org to view the Supplemental Materials.
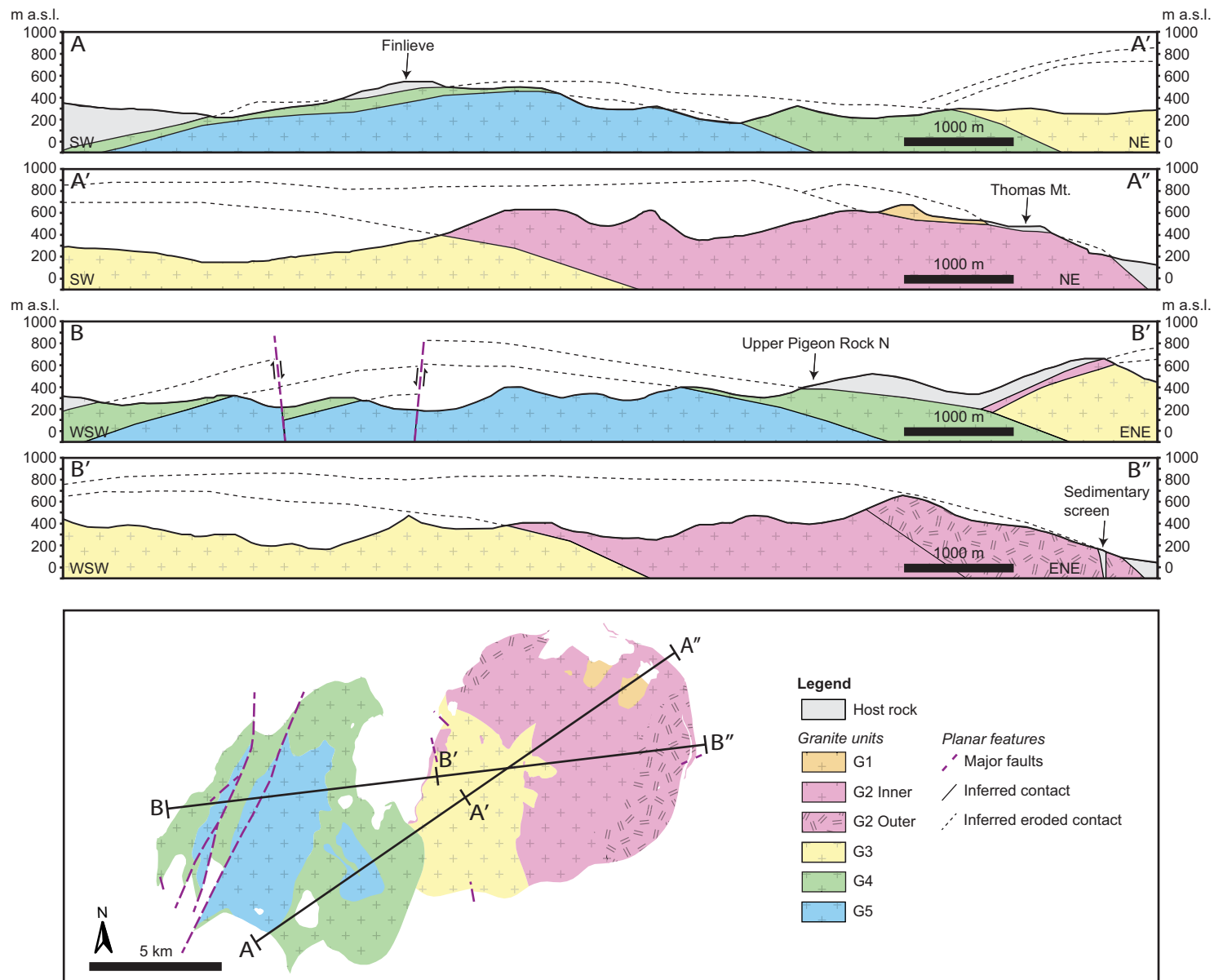
Figure 5. Cross sections showing the granite-host rock and granite-granite contacts of the Mourne granite pluton. The cross sections were created using our observations of contact relationships, the maps and contact observations by Hood (1981) and Gibson (1984) and the topographic surface of the area (Ordnance Survey of Northern Ireland [OSNI] sheets 253–285). Contains public sector information licensed under the terms of the Open Government License v. 3.0. masl—meters above sea level.

3.2. Virtual Outcrops

A virtual outcrop is a georeferenced photomosaic-textured 3D model of an outcrop, which can be used to remotely study structural features, such as fracture orientations (cf. Senger et al., 2015). To examine the fracture pattern near the granite-graywacke contact, we applied structure from motion (SfM) photogrammetry on the host rock to the Western Mourne pluton. Three localities with exposed outcrops at different vertical and horizontal distances to the graywacke-granite contact were chosen as targets for photogrammetry to generate the virtual outcrops.

We performed photogrammetry on nine outcrops in total. Photographs were taken with a 24-megapixel DSLR camera with GPS. We also implemented ground control points, the XYZ (UTM) coordinates of which were saved with a hand-held GPS. One photograph was taken with the camera at chest height and one above the head every meter along the outcrop length. The camera was kept level at an equal distance to the rock face (allowing a fixed focal distance). The images were then processed using the software Agisoft Photoscan™ (http://www.agisoft.com/). The quality of photographs was checked with the function "Estimate Image Quality," and photographs with a quality <0.5 were removed from the image set. First, the photographs were automatically aligned, and tie points in the photographs were identified. The tie points were then used to calculate a point cloud and a mesh surface. The mesh surface was draped with a photomosaic texture created from the photographs generating a 3D "virtual" outcrop. The virtual outcrops were georeferenced using the location information in the metadata of the photographs and the ground control points. In situ fracture measurements were collected at every locality to check the accuracy of the virtual outcrop fracture measurements.

3.3. Three-Dimensional Reconstruction of the Mourne Mountains Granite Pluton Roof

Determining the shape of the roof and wall contacts of the intrusion is important to the understanding of its emplacement (e.g., Burchardt et al., 2010). For example, the dip of the contact should represent the degree of rotation of the host if the intrusion was emplaced by laccolith inflation (e.g., Gilbert, 1877). Since not all contacts could be measured in situ, we used the software MOVE 2017.2™ to perform map analysis for reconstruction of the orientation of the roof contact to the Mourne granite pluton. A topographical surface of the Mourne Mountains was created from the Ordnance Survey of Northern Ireland (OSNI) open data digital-terrain model (sheets 253–285, 10 m resolution, http://www.nationalarchives.gov.uk/doc/open-government-licence/version/3/). The contacts of the Mourne granites from the geological maps of Hood (1981) and Gibson (1984) were traced manually using the line tool in MOVE™ and projected onto the topographical surface. Contact dip data were compiled from previously published data (Hood, 1981; Gibson, 1984), our new field measurements, and structure contours (i.e., the projected contact line). The

dip of the contact was then projected as a surface (down-dip) from the contact line. To reconstruct the shape of the Mourne granite pluton's wall and roof, 14 cross-sections were created in an E-W direction and 23 cross sections in an N-S direction. In each cross section, a line representing the intrusion roof was drawn manually taking into consideration the projected dip of contacts and topography, i.e., where the pluton roof was eroded, the contact was assumed to lie close to the granite peaks to avoid overestimating the dip of the contact (Fig. S2 [footnote 1]). A roof surface of the pluton was created with the Ordinary kriging method using the contacts and the cross-section lines. The dip of the roof surface near the present-day contacts and the roof pendant is well constrained by in situ measurements and by map analysis. However, the shape of the Mourne granite pluton roof far from a present-day exposed contact is uncertain.

3.4. Fracture Orientation Analysis

Fracture measurements were sorted into 16 host-rock localities to discern variability in the fracture pattern around the pluton, as well as one locality with measurements of fractures collected farther than two kilometers from the granite contact (Fig. 2B). The host-rock fracture localities were defined based on measurement location and contact orientation. Fourteen of the localities are located in the pluton roof, where the host rock overlies the granite, and two localities are located in the intrusion wall, where the host rock is laterally adjacent to the granites. Data from the localities were analyzed with k-mean cluster analysis in the software SG2PS (Sasvári and Baharev, 2014). The software was used to separate fracture sets with k-mean clustering, which limits some of the bias in determining which fractures belong to the same set. We used the Fisher k values generated in MOVE™ to determine dispersion within the fracture clusters. Higher Fisher k values indicate a more narrowly clustered set of fractures (Fisher et al., 1993). Fracture data were plotted using the Software Stereonet 10 (Allmendinger et al., 2012). Strike data are given in the right-hand rule convention, i.e., strike is oriented 90° anti-clockwise from the dip direction. The mean principal orientation of a fracture set was calculated in MOVE™. The mean principal orientation is determined by the maximum eigenvector of the poles to the fractures of a set and therefore gives a good estimate of the mean orientation of bimodal data (cf. Mardia, 1975; Fisher et al., 1993).

3.4.1. Virtual Outcrop Analysis and Scan Lines

To analyze the strike and dip (3D orientation) of fractures on the virtual outcrop, the textured surface was imported into the LIME v. 1.0 software (Buckley et al., 2019, http://virtualoutcrop.com/lime) in a local coordinate system, but with accurate scale and orientation. The "Structural data from 3 points" tool was used on the outcrop surface to attain the orientations of measurable

fractures. Fracture orientations in the virtual outcrops were analyzed using (virtual) scan lines in MOVE™, which enable comparison of fracture intensity and spacing between different areas around the pluton (cf. Zeeb et al., 2013). The scan lines were drawn manually with a start and end point placed horizontally along the long axis of the virtual outcrop. Fracture intersections on the scan line were collected by converting the scan lines to wells and counting plane intersections on the well track. Fracture spacing was analyzed with 1 m moving windows in MATLAB™. When measuring fractures along a scan line, a bias is inherently introduced due to the orientation of the scan line. To correct for this bias when comparing fracture intensities between scan line localities, we applied a weighting factor (*w*) (Equation 1):

$$w = \frac{1}{(\sin 90 - \beta)}, \tag{1}$$

where β is the angle between the pole of the fracture and the azimuth of the scan line (Terzaghi, 1965). When the angle between the pole to the fracture and the scan line was ~75°, we did not apply the weighting factor to avoid large and possibly unrepresentative weighting factors (cf. Terzaghi, 1965; Park and West, 2002; Lato et al., 2010).

■ 4. RESULTS

4.1. Contact Relationships to the Mourne Granite Pluton

The exposed contacts between the granite and the Silurian graywacke in the eastern Mourne Mountains are sharp and straight (Figs. 4B–4D). Host-rock xenoliths and granitic dikes intruding the host rock are rare in the eastern part of the Eastern Mourne pluton. However, granitic dikes are common in the host rock on Slieve Muck, next to the western part of the Eastern Mourne pluton. The contact between the host rock and the Western Mourne pluton is sharp and generally either wavy or stepped. Centimeter to decimeter in diameter angular host-rock xenoliths occur abundantly in the granite (Fig. 4D), and granitic veins and/or dikes often intrude bedding and preexisting fracture planes within 50 m from the contact. The internal granite-granite contacts are sharp. G1 displays conjugate fractures above the contact with G2 (Fig. 4F), and the G2-G3 granite contact is wavy at several localities (Fig. 4G).

4.2. Structures in the Contact-Metamorphic Aureole to the Mourne Granite Pluton

The following sections present descriptions of samples collected along traverses in the contact-metamorphic aureole to the Mourne granite pluton (Fig. 2A). See Table S1 (footnote 1) for detailed descriptions of the samples collected in the aureole.

4.2.1. Tollymore Traverse

The Tollymore traverse extends from 100 m to 1660 m north of the granite (Fig. 2A). The rocks in the traverse consist of siltstone and shale altered to hornfels. In sample TM-3, ~60 m from the granite-graywacke contact, diopside and biotite are separated in different layers in the rock. In samples TM-1 and 2 (~700 m from the contact), actinolite and tremolite form layer-parallel segregations that are cut and displaced along chlorite-filled veins (Fig. 6C). In samples >1000 m from the granite-graywacke contact (e.g., TM-7), chlorite and actinolite veins cut the diopside, actinolite, and biotite groundmass of the sample.

4.2.2. Bloody Bridge River Traverse

The Bloody Bridge River traverse extends from the sedimentary screen to 610 m east of the granite contact (Fig. 2A). The samples in the traverse consist of siltstone altered to hornfels. In samples collected in the sedimentary screen and next to the granite-graywacke contact (SC-1, BBT-4, 5, and 8), the groundmass is relatively fine grained compared to samples collected farther from the contact in the traverse (BBT-9–16). Samples SC-1 and BBT-8 display diopside segregations, and samples BBT-4 and 5 display diopside and actinolite segregations that are cut by quartz and actinolite veins. The sedimentary screen samples are either brecciated or folded (Fig. 6B), and sample BBT-3 has an intrusive breccia vein (tuffisite with cataclasite texture) with biotite-rich hornfels and feldspar clasts (Fig. 6A). The granite to the west of the sedimentary screen in the eastern part of the Eastern Mourne pluton is also brecciated and displays several millimeters to centimeter thick contact-parallel cataclasite bands (Fig. 4E). In sample BBT-12 (~100 m from the contact), diopside segregations are cut by thin quartz veins, which are transgressed by quartz and actinolite veins. Sample BBT-14 (~210 m from the contact) is brecciated, and biotite and quartz segregations are displaced by fractures. Sample BBT-16 (~610 m from the contact), located in the far end of the traverse, shows bedding-parallel diopside and actinolite segregations.

4.2.3. Glen River Traverse

The Glen River traverse extends from 100 m to 770 m NE of the granite contact (Fig. 2A). The rocks in the traverse consist of siltstone but also shale altered to hornfels. Porphyroblasts of amphibole (likely kaersutite) and actinolite have crystallized in the biotite-dominated groundmass of sample GRT-4, which is transgressed by quartz and diopside segregations. In the samples collected farther than 200 m from the granite-graywacke contact, the porphyroblasts disappear, but plagioclase, quartz, and diopside segregations are still present in the rock and are cut by later quartz veins. The samples GRT-10–15 in the far end of the traverse are banded (Fig. 6D). In the darker layers, the quartz is clotted, while quartz clasts are more abundant in the lighter layers of the hornfels. The

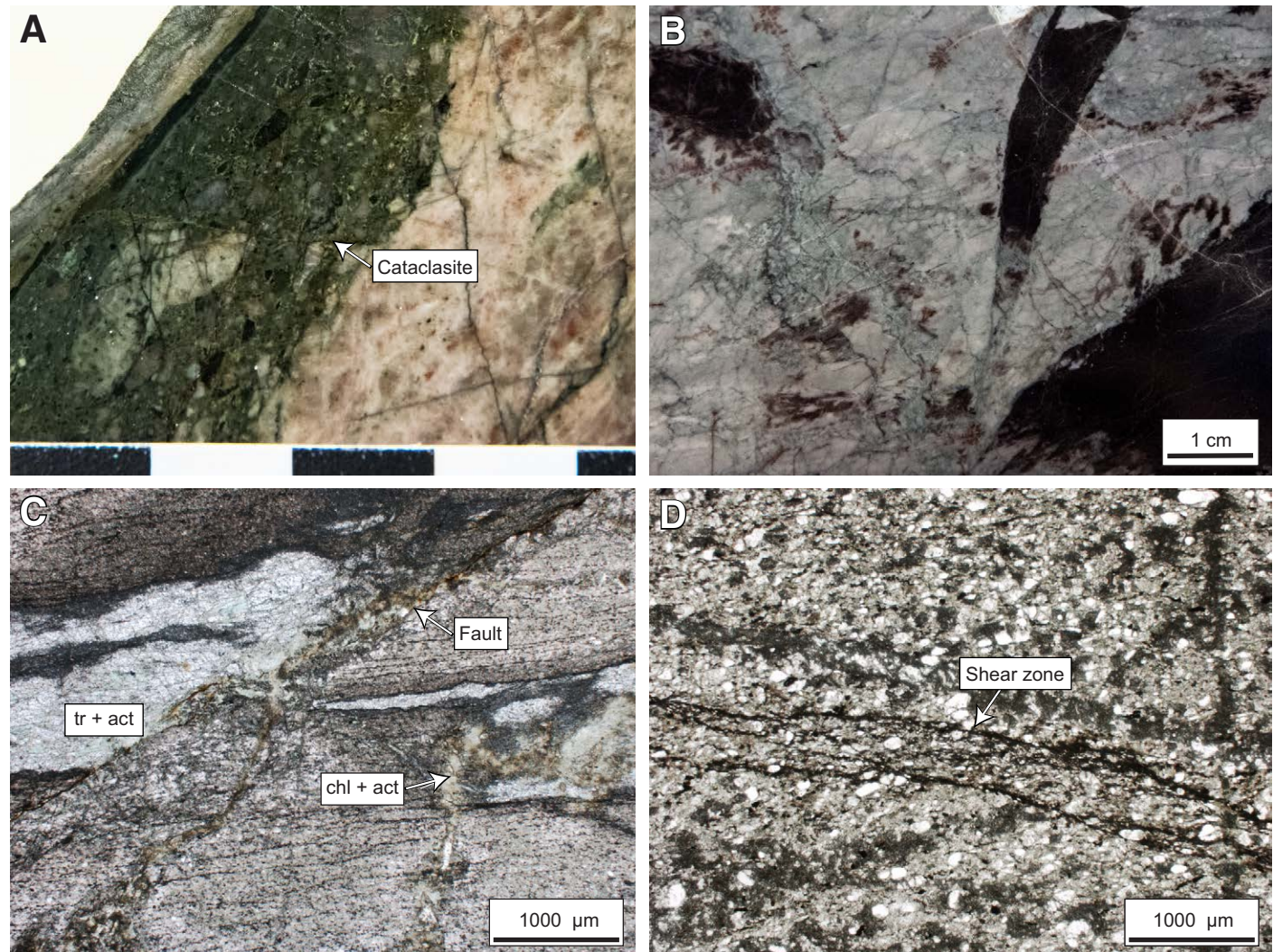Mattsson et al. | Emplacement of the Mourne granite pluton

Figure 6. (A) Sample BBT-3: Tuffisite with cataclasite texture from the sedimentary screen with green groundmass, feldspar (light), and biotite-rich siltstone (dark) clasts. Fields on the scale are 1 cm long. (B) Sample BBT-5: Breccia in the sedimentary screen with light diopside and dark biotite-rich remnant siltstone clasts. (C) Sample TM-1 (PPL): Bedding-parallel tremolite (white) and actinolite (light-green) segregations in fine-grained graywacke collected ~700 m from the granite contact. A fault displaces the tremolite and actinolite segregations and is filled with chlorite (green mineral). (D) Sample GRT-15 (PPL): Cataclasite shear zone in hornfels located ~770 m from the granite-graywacke contact. The groundmass in the lighter parts consists of diopside and actinolite, while the groundmass in the darker parts consists of clotted quartz, biotite, oxides, and plagioclase. Mineral abbreviations: act—actinolite; chl—chlorite; tr—tremolite.

Mattsson et al. | Emplacement of the Mourne granite pluton

layers are displaced (≤1 mm) along fractures. Several thin cataclasite shear zones occur parallel to the layers (Fig. 6D), and GRT-13 and 15 are brecciated.

4.2.4. Roof Sample

In a siltstone (hornfels) sample from Shan Slieve (SS-1) next to G1, the groundmass is biotite-rich and cut by quartz veins, diopside segregations, and quartz and actinolite veins. Within a shear zone, both amphibole and sigmoidal porphyroblasts are replaced by quartz, biotite, and alkali feldspar. The mineral assemblage suggests that the retrogressed porphyroblasts were originally cordierite (cf. Pattison and Tracy, 1991).

4.3. Bedding Orientation and Roof Shape Reconstruction

The inclination of the graywacke bedding varies in the Mourne Mountains, ranging from subhorizontal to subvertical (8°–88°) with an average dip of 29° and a mean principal plane that strikes 054° (Table 1; Fig. 7). Several open folds are observed in the host rock on Slieve Muck (cf. Richey, 1927; Hood, 1981). The reconstructed fold axis of the folds on northern Muck trends 238/21°, and on southern Muck, the reconstructed fold axis trend and plunge 229/21°. The reconstructed axial surfaces of the folds at different localities are also similar with orientations of 226/62° on northern Muck and 218/71° (strike/dip) on southern Muck, respectively. The reconstructed roof of the Eastern Mourne granite pluton is slightly dome shaped (Figs. 5, 8A, and 8B; Fig. S1 [footnote 1]), and the edges of the pluton roof dip shallowly to moderately outwards from the center of the pluton (~10°–50°) (Figs. 8C and 8D). Map analysis indicates that the roof to the eastern part of the Western Mourne pluton dips shallowly (~10°) to the east and suggests that the inclination of the roof to the western part of the Western Mourne pluton is marginally steeper inclined (~15°) (Figs. 5, 8C, and 8D; Fig. S1).

4.4. Fracture Pattern

In total, 4549 measurements were collected on structural features including contacts, bedding, fractures, dikes, and lineaments in the Mourne Mountains and the surrounding area. The data for fractures, dikes, and lineaments are presented below and in Supplemental Table S2 (footnote 1).

4.4.1. Regional Fractures

In total, 505 lineaments interpreted to represent faults and fractures were remotely measured on beach exposures of the Hawick Group east of the Mourne Mountains (Fig. 1B and Supplemental Fig. S3). The measured linea-

ments trend primarily 140° and secondarily 035°. Measured lineaments interpreted to represent bedding trend on average 060° (*n* = 88). Orientations of fracture and bedding lineaments on beach exposures adjacent to the Mourne Mountains are offset compared to lineaments measured >10 km from the intrusion, where the fracture and fault lineament sets trend 100° and 160°. All fracture data are given in Supplemental Table S2 (footnote 1).

4.4.2. Fractures in the Intrusion Roof

In total, 2094 fractures were measured in host-rock outcrops surrounding the Mourne granite pluton (Fig. 9A). Four subvertical fractures sets are observed in the studied roof outcrop localities striking dominantly SE, S, NE, and E (see Table 1 for detailed orientation of each fracture set; Figs. 2B, 4B, and 10A). It was only possible to distinguish a maximum of three sets of subvertical fractures at a single locality, which could be due to outcrop orientation. In several localities, a set of subhorizontal fractures is also identified. In the southwestern part of the Western Mourne pluton, the dominant strike of the subvertical fracture sets is NW, N, and E. There, the calculated mean principal fracture plane of the NW(-SE)–striking fracture set dips toward the NE as opposed to the SW, which is the dominant dip-direction in the other studied localities (Table 1). Limited fracture plane exposures made it hard to observe slickenlines or other displacement indicators. All fracture data and k-mean cluster groupings are given in Supplemental Table S2 (footnote 1).

4.4.3. Fractures in the Intrusion Wall

In the wall rock to the Mourne granite pluton at Glen River (Fig. 2A), the mean strike of the bedding is 298°, and two dominant fracture sets were identified striking 209° and 271° (Table 1; Figs. 7 and 10A). In the Bloody Bridge River, the mean strike of the bedding is 017°, and two fracture sets were identified that strike 165° and 274° (Table 1; Figs. 7 and 10A). All fracture data and k-mean cluster groupings are given in Supplemental Table S2.

4.4.4. Joints in the Granites

In total, 1411 fractures were measured within the Mourne granite pluton (Fig. 10B). We determined these fractures to overwhelmingly be joints since displacement could rarely be observed on them (cf. Pollard and Aydin, 1988). The G1 joints were studied at three different localities and are primarily subvertical and dip toward the S and SW. The jointing in G1 is visibly denser spaced compared to the more voluminous younger granites. Conjugate fractures with moderate dips were observed in the easternmost studied outcrop of G1. A subhorizontal set of joints in G1 was also identified; the set dips on average 20° (*n* = 30) to the NNE (Fig. 10B).

TABLE 1. STRUCTURAL DATA FROM THE DIFFERENT STUDIED HOST-ROCK LOCALITIES

Roof rock	Location	SUDL*	Lower Pigeon Rock	Upper Pigeon Rock S	Upper Pigeon Rock N	Spelga Mountain	Slievenamiskan	Cock Mountain	Finlieve	Gruggandoo	Slievemiskan
Contact orientation	**Strike**	-	25	265	199	334	29	12	125	223	84
	Dip	-	12	3	4	22	15	8	11	24	15
Distance from contact	**Horizontal (m)**	>2000	10	0	~400	~70	1 to 50	<40	10 to 300	5 to 250	~40
	Vertical (m)	-	<10	<5	<100	~40	<10	<10	10 to 20	<100	<10
Bedding orientation	*n*	102	10	6	1	11	7	1	13	7	10
	Azimuth	144	87	320	133	119	157	199	319	227	335
	Dip	89	18	14	43	41	84	45	86	11	84
Fracture set 1 (mean principal plane)	*n*	260	60	30	37	24	80	18	77	150	119
	Azimuth	242	242	235	236	60	240	228	53	57	53
	Dip	90	89	85	88	86	89	89	55	77	85
	Fisher k	1.05	1.32	2.09	1.18	1.58	1.38	1.21	3.26	2.75	1.38
	Two-variable Fisher k	7.89	25.80	20.38	37.37	36.50	24.60	22.55	10.20	17.41	12.31
Fracture set 2 (mean principal plane)	*n*	182	24	27	28	27	39	29	34	66	43
	Azimuth	305	280	90	126	113	280	274	100	108	349
	Dip	88	74	84	81	87	88	88	86	86	88
	Fisher k	1.05	5.46	1.35	1.80	1.47	1.31	1.37	1.43	1.43	1.35
	Two-variable Fisher k	11.36	43.20	33.87	7.37	15.41	12.08	11.94	14.06	16.46	6.71
Fracture set 3 (mean principal plane)	*n*	-	18	54	16	54	58	31	23	110	26
	Azimuth	-	177	168	357	352	333	181	178	179	103
	Dip	-	84	90	83	88	83	86	88	82	87
	Fisher k	-	1.24	1.19	2.14	1.28	1.48	1.36	1.42	1.68	1.32
	Two-variable Fisher k	-	4.99	8.82	5.06	5.86	10.43	8.86	4.94	5.96	16.57

Roof rock	Location	Slieve Muck S	Slieve Muck N	Tollymore	Thomas Mt. and Shan Slieve	Eastern roof cappings	Wall rock	Glen River	Bloody Bridge River
Contact orientation	**Strike**	150	211	307	272	12	Strike bedding	298	17
	Dip	22	20	20	19	22	Angle of rotation†	51	-50
Distance from contact	**Horizontal (m)**	<50	<50	50 to 600	80 to 200	~10	Horizontal (m)	0 to 450	0 to 130
	Vertical (m)	<50	<50	<200	<30	~10	Vertical (m)	-	-
Bedding orientation (mean principal plane)	*n*	18	35	10	8	10	*n*	8	6
	Azimuth	187	176	320	344	130	Azimuth	28	107
	Dip	35	38	78	18	36	Dip	40	40
Fracture set 1 (mean principal plane)	*n*	95	43	15	53	15	*n*	29	45
	Azimuth	244	52	233	246	223	Azimuth	299	255
	Dip	88	80	86	83	84.7	Dip	84	76
	Fisher k	1.26	1.48	1.25	1.43	1.87	Fisher k	1.46	2.63
	Two-variable Fisher k	23.07	23.35	21.67	10.56	14.09	Two-variable Fisher k	8.39	13.87
Fracture set 2 (mean principal plane)	*n*	55	37	36	12	38	*n*	22	58
	Azimuth	291	89	129	301	277	Azimuth	1	4
	Dip	81	83	87	78	78	Dip	88	89
	Fisher k	1.54	1.75	1.31	2.73	1.67	Fisher k	1.36	1.53
	Two-variable Fisher k	11.14	22.03	4.79	25.09	16.58	Two-variable Fisher k	17.41	6.41
Fracture set 3 (mean principal plane)	*n*	54	90	31	13	-			
	Azimuth	346	305	185	1	-			
	Dip	89	85	81	89	-			
	Fisher k	1.39	1.68	2.06	1.98	-			
	Two-variable Fisher k	14.49	19.83	7.81	22.53	-			

*Southern Uplands–Down-Longford terrane.
†Difference between the regional trend of bedding (067°, Anderson, 1987) and the bedding trend at the locality.

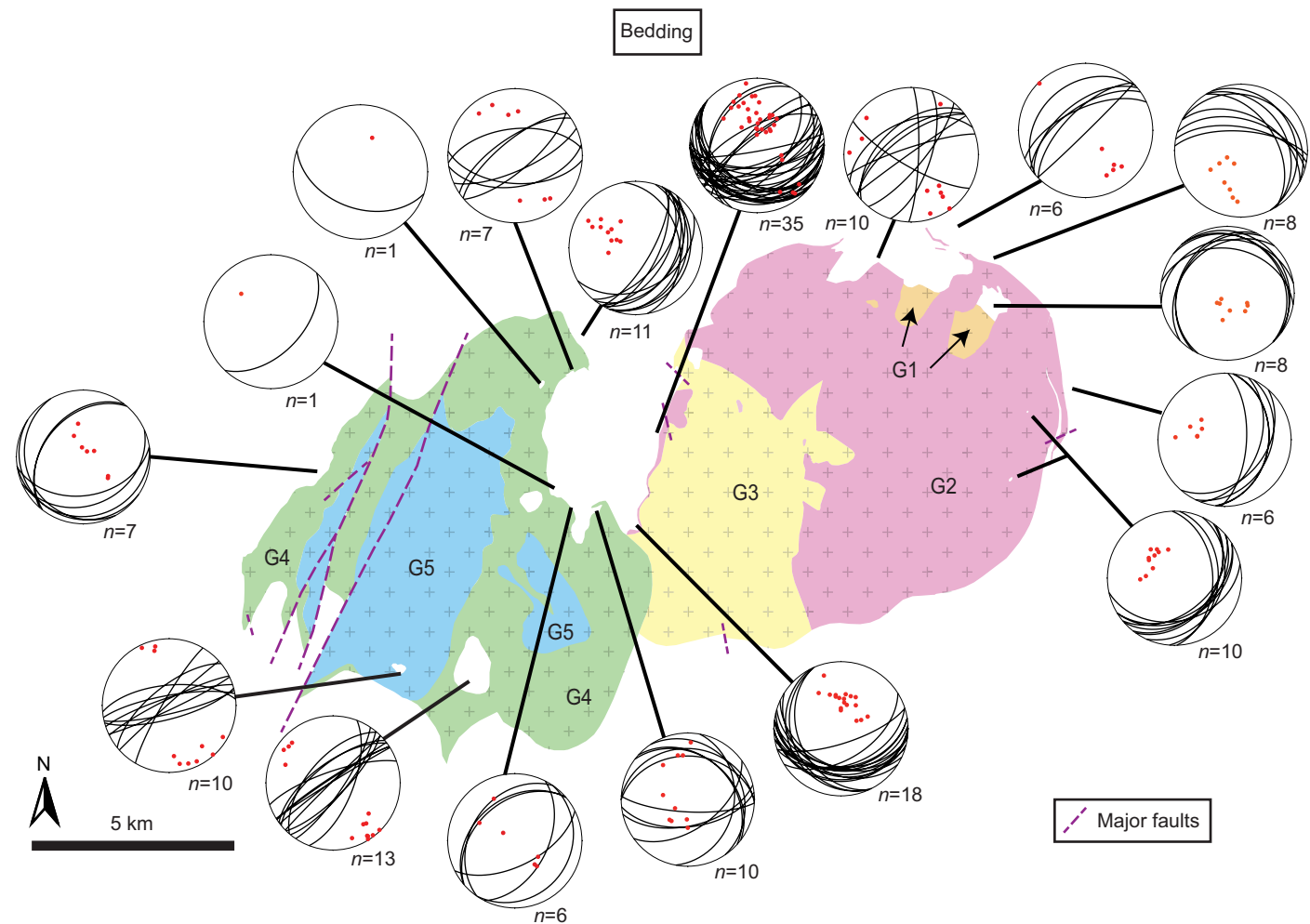Mattsson et al. | Emplacement of the Mourne granite pluton

Figure 7. Planes and poles to bedding at each host-rock fracture study locality plotted in lower-hemisphere Schmidt stereonets. The map of the Mourne granite pluton is redrawn after Hood (1981) and Gibson (1984).

The studied outcrops of G2 and G3 in the central part of the Eastern Mourne pluton have similar joint sets with two subvertical joint sets striking SW and ESE and a subhorizontal set of joints. At Bloody Bridge River, a pervasive set of subvertical joints in G2 outer strikes to the S. At Glen River, joints in G2 are steep and dip dominantly to the SW. The G4 joint pattern is similar to those of G2 and G3 and includes subvertical and subhorizontal joint sets. At Gruggandoo, two steeply inclined joint sets occur in G4; these sets strike NW and NE (Fig. 10B). Next to the granite-graywacke contact, a set of fractures in G4 is oriented 319/80° ($n = 20$). Four striations were measured on the fracture surfaces, which trend and plunge 135/37° on average. The G5 joint pattern largely resembles the G4 joint pattern (Fig. 10B). All joint data are given in Supplemental Table S2 (footnote 1).
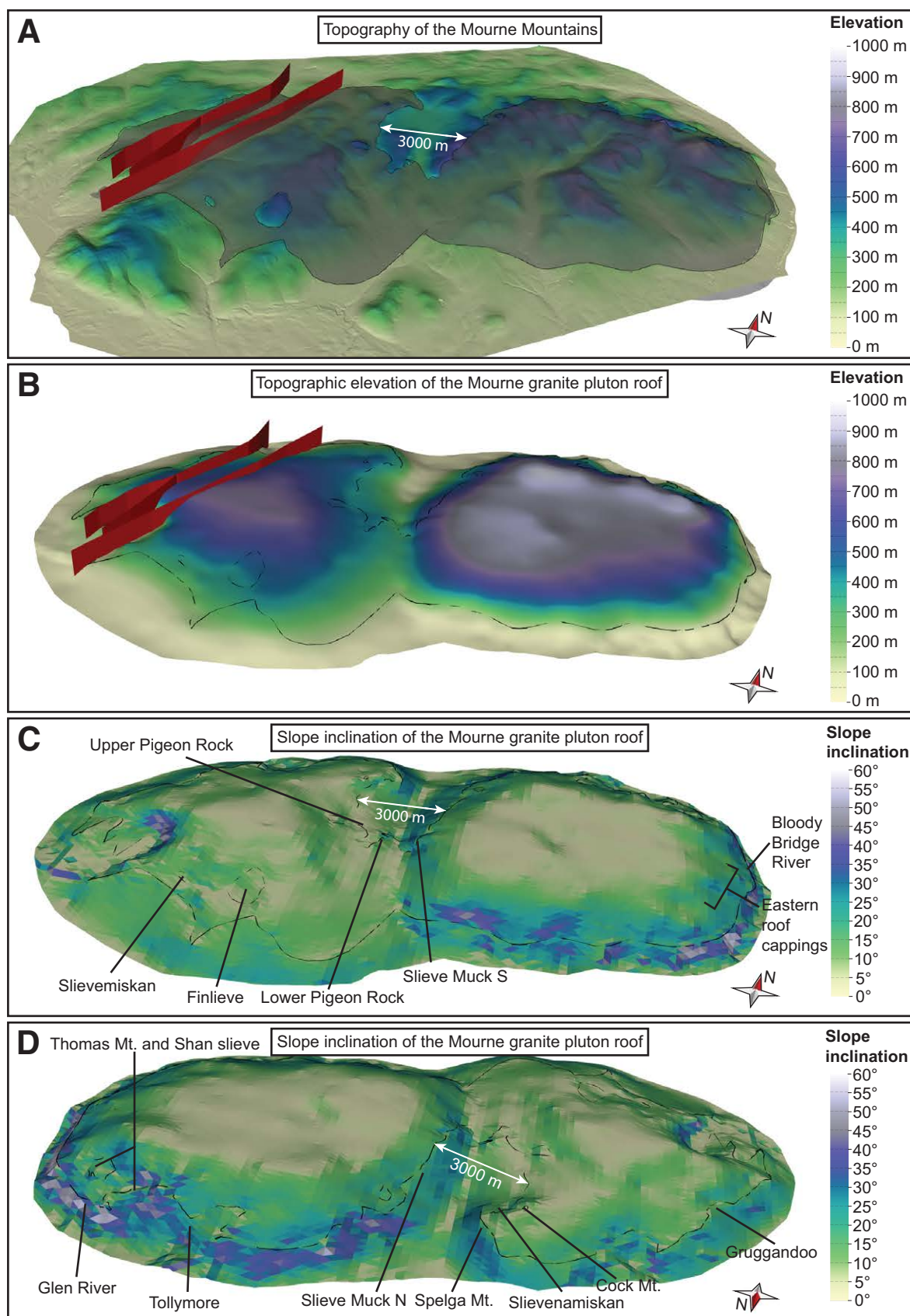
Figure 8. Topography of the Mourne Mountains (Ordnance Survey of Northern Ireland [OSNI] sheets 253–285, contains public sector information licensed under the terms of the Open Government License v. 3.0). (A) Reconstructed roof surface of the Mourne granite pluton (A–D) highlighting topographic elevation (A and B). Slope inclination of the reconstructed roof surface is shown in C and D. Regional faults are visualized by the red planes. (B) Reconstructed roof surface of the Mourne granite pluton colored after elevation. (C) Perspective view from SSE and (D) perspective view from NNW of reconstructed roof surfaces of the Mourne granite pluton. Colors show slope inclination. The black line on the surfaces marks the present-day contact between the granite and host rock. The extent of the Mourne granite pluton at depth is unknown; these surfaces represent only the roof and the upper part of the wall to the pluton. The host-rock fracture-study localities are also indicated on the map.
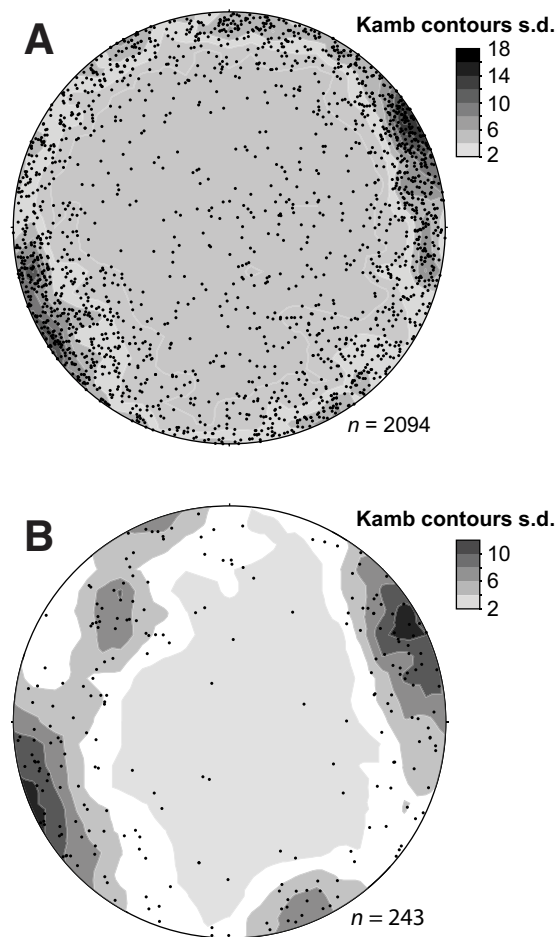
Figure 9. Poles to planes of (A) all in situ–measured fractures and (B) the granitic dikes in the host rock to the Mourne granite pluton plotted in lower-hemisphere contoured Schmidt stereonets. The stereonets were contoured with Kamb contouring with a contour interval of 2σ and a significance level of 3σ. s.d.—standard deviation.

4.4.5. Granitic Dikes

In total, 243 granitic dikes that range from decimeter to millimeter in thickness were measured in the host rock to the Mourne granites (Fig. 9B). The granitic dikes in the Mourne Mountains parallel the fractures in the host rock and strike dominantly SE and secondarily S and NE (Fig. 9B). All dike data are given in Supplemental Table S2.

4.5. Scan Lines

The weighted (bias-corrected) average fracture intensity on the studied scan lines ranges from 2.2 to 5.5 fractures/m, while the uncorrected fracture intensity ranges from 0 to 11 fractures/m in the studied outcrops. Scan line locations are given in Figure 10A; see Figure 11 and Table 2 for results and Supplemental Table S3 for weighting factors of individual fractures collected on the scan lines and the supplementary information for individual scan line data. The scan lines show that the NW-striking fracture set is the most dominant set in the host rock. This is corroborated by relatively low fracture intensity observed along the scan lines at Pigeon Rock; these lines trend toward the NW and are roughly parallel to the NW-striking fracture set. The scan lines record no distinct decrease in fracture intensity with distance from the contact (Fig. 11; Table 2). Fracture intensity may instead be controlled by lithology in the Hawick Group (cf. Anderson, 1987). However, our data cannot resolve this further. The fracture data collected on the virtual scan lines compare well with the data measured in situ at the scan line localities (albeit not along a scan line) (see Supplemental Fig. S4).

■ 5. BRITTLE DEFORMATION FEATURES IN AND AROUND THE MOURNE GRANITE PLUTON

5.1. Joint Orientations in the Granites

G1 exhibits a conjugate set of fractures (Fig. 4F), which suggests that G1 was deformed in a brittle manner when G2 intruded or at separate deformation event. The highly systematic vertical and subhorizontal fractures in G2 to G5 are interpreted as cooling joints (cf. Cloos, 1922; Price and Cosgrove, 1990). In the Eastern Mourne pluton, the subvertical joints that strike parallel to the internal contacts (G1-G2 and G2-G3) dip toward the SW. Cooling joints in magmatic intrusions are generally oriented at a high angle to the contacts (cf. Cloos, 1922; Price and Cosgrove, 1990; Bergbauer and Martel, 1999) and therefore support the interpretation that the external and internal contacts in the Eastern Mourne pluton dip at a shallow angle toward the NE (Fig. 5; see also section 2.3.1; Hood, 1981). Moreover, the subhorizontal joints dip dominantly toward the NE. In the Western Mourne pluton, the orientation of the subhorizontal and subvertical joints are largely parallel and perpendicular to the orientation of the host-rock contact (Fig. 10B), respectively, which is inclined outward from the center of the Western Mourne pluton (cf. Figs. 8B–8D).

5.2. Fractures in the Host Rock to the Mourne Granite Pluton

Three possible scenarios can be envisaged regarding the timing of the different fracture sets in the host rock to the Mourne granite pluton. The fractures either (1) pre-date, (2) formed syn-emplacement, or (3) post-date the emplacement of the granites. We now discuss how to evaluate the timing
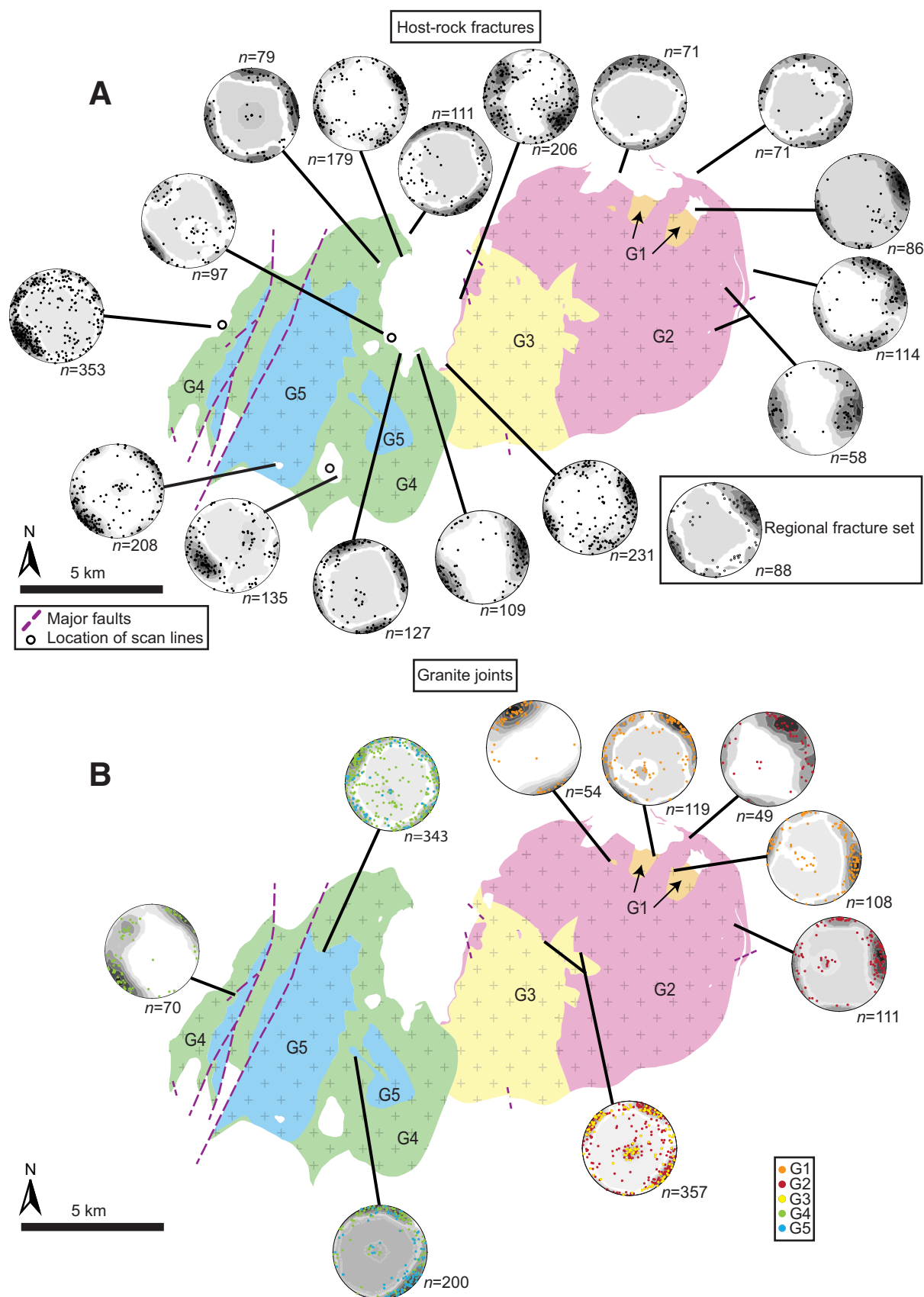
Figure 10. (A) Poles to fracture planes from each host-rock fracture-study locality plotted in lower-hemisphere contoured Schmidt stereonets. The fracture-study localities are shown on the map of the Mourne granite pluton. (B) Poles to joints in granite from different areas in the Mourne pluton plotted in lower-hemisphere contoured Schmidt stereonets. The stereonets were contoured with Kamb contouring with a contour interval of 2σ and a significance level of 3σ.
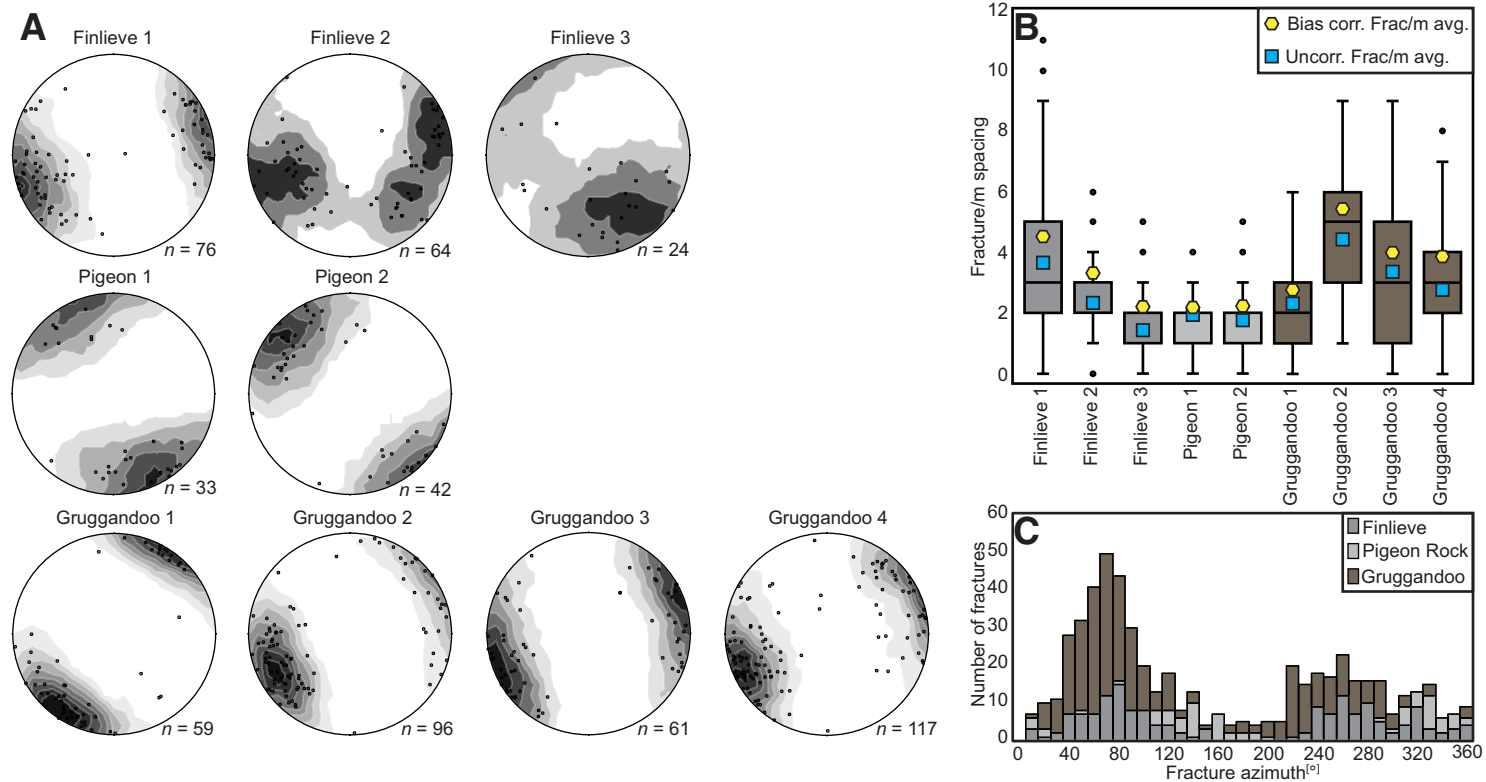
Figure 11. (A) Poles to uncorrected scan line fractures at the respective locality plotted in lower-hemisphere Schmidt stereonets. The stereonets were contoured with Kamb contouring with a con-
tour interval of 2σ and a significance level of 3σ. The orientation of the fractures on the scan lines is similar where the scan lines trend in approximately the same direction (e.g., Finlieve 1 and 2,
Gruggandoo 1–4; Table 2). (B) Scan-line whisker plots of uncorrected fracture spacing at the different studied outcrops. Fracture intensity was analyzed with a 1-m-wide moving window. (C) Stacked
histogram showing uncorrected fracture orientation frequency at the different scan-line localities. The Pigeon Rock fracture orientation distribution differs from the two other areas, which is most
likely due to the approximately NW-SE orientation of the scan lines. This orientation is parallel to the most abundant set of fractures at Finlieve and Gruggandoo. The fracture intensity is higher at
NE-striking outcrops, which suggests that the observed fracture intensity is strongly dependent on the orientation of the outcrop and not the distance to the granite contact.

of formation of the fractures measured in the Mourne granite pluton and its host rock.

(1) The Southern Upland–Down-Longford terrane records both ductile and brittle deformation phases associated to the Caledonian orogeny (Anderson and Cameron, 1979; Anderson, 1987). The recorded regional fracture orientations overlap with the three sets of strike-slip faults recorded by Anderson (1987) on the Ardglass peninsula that strike dominantly 195°, 355° and 125°. However, our fracture data present different dominant orientations. Fractures measured farther than 2 km from the granite contact and remotely measured lineaments on the coast NE of the Mourne granite pluton strike SE and SW (Table 1; Figs. 1B and S3 [footnote 1]).

Notably, the remotely measured regional fractures show strong correlation with two of the measured fracture sets in the host rock to the Mourne granite pluton (Table 1).

(2) Fractures related to the emplacement of shallow magmatic intrusions are commonly parallel or perpendicular to the intrusion contact (Johnson and Pollard, 1973; de Saint-Blanquat et al., 2006; Morgan et al., 2008; Feng et al., 2011; Wilson et al., 2016). Wilson et al. (2016) also reported later tensile joints in the host rock to the Trachyte mesa intrusion in the roof and at the margins that are parallel and perpendicular to the intrusion margin and interpreted them to be related to extension during the final stage of magma emplacement. In the roof to the Black Mesa pluton, USA, steeply

TABLE 2. SCAN-LINE DATA

Scan-line name	Scan-line coordinates Decimal degrees WGS84		n scan-line segments	Scan-line orientation		Total length (m)	Number of fractures	Fractures/ m avg.	Bias-corrected fractures/m avg.
	Latitude	Longitude		Trend*	Vertical distance to granite contact (m)				
Finlieve 1	54.108632	−6.111789	2	243	10	20.8	76	3.7	4.5
Finlieve 2	54.110901	−6.108820	3	255	20	27.2	64	2.4	3.3
Finlieve 3	54.118284	−6.10759	1	130	15	16.5	24	1.5	2.2
Gruggandoo 1	54.157344	−6.168094	3	219	40	25.3	59	2.3	2.8
Gruggandoo 2	54.159263	−6.165141	3	243	50	21.6	96	4.4	5.5
Gruggandoo 3	54.161016	−6.163558	2	75	60	18.1	61	3.4	4.0
Gruggandoo 4	54.161431	−6.164636	3	63	80	41.7	117	2.8	3.9
Pigeon 1	54.154701	−6.076942	2	146	15	16.9	33	2.0	2.2
Pigeon 2	54.156436	−6.073939	3	143	35	23.3	42	1.8	2.3

*Scan lines are horizontal, mean orientation of segment azimuths.

inclined joints are oriented perpendicular to the direction of strain (flow of magma) during magma emplacement (de Saint-Blanquat et al., 2006). Additionally, the fracture intensity has been reported to increase towards the intrusion contact (Woodcock and Underhill, 1987; de Saint-Blanquat et al., 2006; Morgan et al., 2008; Wilson et al., 2016). We therefore assume that fracture sets created by deformation during the emplacement of the Mourne granite pluton should be parallel and perpendicular to the pluton contacts. This is supported by the orientation of the joints within the Mourne pluton, which indicates extensional stresses parallel and perpendicular to the contact (see section 5.1.; Fig. 10B). In contrast, the orientations of the steeply inclined fracture sets in most roof outcrops around the Mourne granite pluton are strikingly similar, even where the strike of the contact is different (see Fig. 10A and Table 1 for a comparison of the fracture sets at the different studied host-rock localities). For example, at localities where the contact between granite and host rock dips >20°, such as on Shan Slieve and Thomas Mountain, next to G1, the fractures dip steeply and with orientations similar to the regional fracture sets. Also, on Southern Slieve Muck, where the contact dips >20°, the fracture sets are steep with strikes similar to the regional fracture sets. Moreover, the scan lines show that observed fracture pattern differences (for example, between the Pigeon rock and Gruggandoo scan lines) are most likely due to the orientation of the studied outcrops (see section 4.5; Fig. 11; Table 2). Additionally, the scan lines do not record a decrease in fracture intensity with increasing distance from the granite contact and exhibit quite consistent fracture orientations (Fig. 11; Table 2). These observations suggest that the most dominant fracture sets in the host rock to the Mourne pluton formed before the emplacement of the granites. However, at localities where the roof is relatively flat (e.g., Upper Pigeon rock, ~4°W) some fracturing might have been caused by magma flow. The magnetic fabric close to the Pigeon Rock localities in-

dicates flow toward the NE (Stevenson and Bennett, 2011), roughly perpendicular to the strike of the contact and the SE-striking dominant fracture set. The wall-rock outcrops at Bloody Bridge and Glen River show roughly contact-parallel and contact-perpendicular fracture orientations, which imply that these fractures could have formed during granite emplacement. Additionally, the mean orientation of the dominant fracture set in the scan line Gruggandoo 1 (312/79°, n = 65) is parallel to fractures in granite G4 (319/80°, n = 20), located just below the granite-graywacke contact at Gruggandoo. Both fracture sets strike perpendicular to the contact. The striations on the G4 fractures indicate displacement parallel to the dip direction of the contact. The other Gruggandoo scan lines do not correlate with the G4 fractures (Fig. 11A). The Gruggandoo 1 scan line might therefore display an emplacement-related fracture set located close to the contact.

(3) Fractures formed after the emplacement of a granite are expected to have similar orientations whether they develop within the granite or the host rock (assuming that the difference in rheology does not have an influence). In our case study, the orientations of the dominant fracture sets in the host rock and joints in the granite do not correlate (Fig. 10). Any abundant postemplacement fracturing in the Mourne Mountains is therefore deemed unlikely.

While a syn-emplacement origin to some of the fractures measured in the roof to the Mourne granite pluton is hard to rule out, the two most dominant SE- and NE-striking fracture sets can be observed in the roof all around the pluton. We therefore assume that these fracture sets formed prior to the emplacement of the granites. The granitic dikes are largely parallel to the most dominant NE-SW–striking fracture set, which shows that the magma intrusion utilized these fractures in the roof. The presence of abundant preexisting fracturing may therefore have inhibited the formation of new fractures in the host rock during emplacement of the Mourne pluton.

5.3. Quantifying Rotational Host-Rock Deformation around the Mourne Granite Pluton

The shallow outward inclination of the granite-granite and granite-graywacke contacts, i.e., the dome shape of the Mourne granite pluton, was proposed by Stevenson et al. (2007) to reflect laccolith inflation (see also Figs. 8C and 8D). Hence, if we assume that the Mourne granites were initially horizontal sills that inflated into laccoliths, the dip of the contact should correspond to the doming of the host rock, i.e., the dip of the contact is the angle of rotation of the host rock caused by up-doming (cf. Fig. 3B).

Our results indicate that the orientation of the bedding at the same locality and between localities where the contact has similar orientation and dip (Fig. 7; Table 1). Moreover, the limited exposure of the host rock combined with the preexisting deformation (see section 2.1.) make the Hawick Group bedding unsuitable to test for up-doming and deformation within roof rock by magma emplacement. Instead, we employ the pervasive regional fracture sets in the host rock that formed prior to or locally during the granite emplacement (see section 5.2) as passive markers. Passive markers are expected to be deformed together with the host rock (cf. Fossen, 2010, p. 62); therefore, the fracture orientations should reflect the dip of the pluton contact if rotational deformation occurred during granite emplacement (Nelson and Sylvester, 1971; Feng et al., 2011).

In order to test if the host rock to the Mourne granite pluton has been deformed by laccolith inflation, we performed rotations of steeply dipping regional fractures and compared these rotated fracture sets with our in situ–measured host-rock fractures and dikes. The scan line data were not used for this comparison. The regional fractures used for the rotation were compiled from fracture data collected at distances of >2 km from the granite pluton. In the host rock to shallowly emplaced laccoliths, emplacement-related deformation can generally only be observed within a couple hundred meters from the lateral boundary of the intrusion (cf. de Saint-Blanquat et al., 2006; Morgan et al., 2008; van Wyk de Vries et al., 2014; Wilson et al., 2016; Mattsson et al., 2018). Laccoliths inflate by uplifting and rotating the host rock on the flanks of the intrusion (e.g., Pollard and Johnson, 1973; van Wyk de Vries et al., 2014). The accompanied rotation of the host rock during laccolith growth should be clockwise around a horizontal axis that trends parallel to the strike of the contact to the pluton. A clockwise rotation would either steepen or shallow regional fractures depending on the relative location on the pluton roof and the orientation of the preexisting fracture sets. The degree of rotation was assumed to be the same as the dip of the roof contact at the different roof localities (see above). To complement the rotation analyses of the regional fractures (Fig. 12; Supplemental Table S4 [footnote 1]), the in situ–measured fracture sets were rotated by subtracting the dip of the contact ("back-rotated") at the respective host-rock locality (see Supplemental Fig. S5).

The results show that the rotated regional fracture sets do not correlate consistently with the measured fractures in the other roof-rock localities around the Mourne granite pluton (Fig. 12; Supplemental Table S4 [footnote 1]). For example, the Southern Slieve Muck, Thomas Mountain, and Slievenamiskan localities do not correlate with the rotated regional fracture sets, which should be the case if the Mourne granites were emplaced as laccoliths. However, at the Gruggandoo locality, the mean principal plane of Fracture set 1 of the rotated regional fractures is oriented 334/89° (strike, Supplemental Table S4) and is similar to the orientation of the mean principal plane of Fracture set 1 of the in situ measured fractures at Gruggandoo (327/77°, strike, Table 1). A similar pattern can also be observed when comparing the in situ–measured fracture sets and the rotated regional sets of the Finlieve and Slievemiskan localities (see section 4.4.2.; Fig. 12; Table 1; Supplemental Table S4). This is consistent with some inflation related to the emplacement of the granite in the western part of the Western Mourne pluton. Although, these fracture patterns require a greater rotation than suggested by the dip of the contact to reproduce the regional fracture pattern (Supplemental Fig. S5).

An inclined and curved geometry of the initial sill(s) (cf. Hood, 1981; Stevenson et al., 2007) could explain the lack of distinct rotation in the roof. For example, if the initial sill(s) was slightly dome-shaped, it would not result in any distinct rotation in the host rock, since the inflation of the sill(s) would be mostly accommodated by vertical uplift of the roof along faults (de Saint-Blanquat et al., 2006; Stevenson et al., 2007, Fig. 12). However, there is no indication that the magma lifted the roof along faults in the southern and western part of the pluton, and the fracture pattern does not suggest a distinct rotation on Slieve Muck in the western part of the Eastern Mourne pluton. On the other hand, if the Western Mourne granites were emplaced as laccoliths with a northeast-ward-inclined floor, the result would be little to no rotation in localities such as Slievenamiskan and Lower Pigeon Rock, while the host rock at Gruggandoo, Finlieve, and Slievemiskan would be rotated.

The wall rock to the Mourne granites, which was studied in the Glen and Bloody Bridge Rivers, reveals two dominantly steeply inclined fracture sets striking 209° and 271° and 165° and 274°, respectively (Fig. 10A; Table 1). This is roughly parallel and perpendicular to the pluton contact and could indicate that these fracture sets formed during the emplacement of the granites (see section 5.2.). However, the dominant SE-striking fracture set observed in the roof outcrops is seemingly absent. We therefore also tested rotating the fracture data collected in the wall to the pluton (Fig. 12). A rotation around a horizontal axis at an angle of ~35 to 50° (dip of contact at the wall localities; see Hood, 1981) markedly shallows the dip of the wall-rock fractures. Such a rotation does not resolve the existence of steeply inclined fracture sets at the Glen and Bloody Bridge River localities (Fig. 10A; Table 1). Notably, rotation of the wall-rock fracture sets around a vertical axis at an angle representing the difference between the regional strike of the bedding (067°, Anderson, 1987) and the strike of the bedding at the studied locality aligns the two dominant fracture sets observed in the wall-rock localities parallel to the dominant SE- and NE-striking regional fracture sets. Furthermore, the "best-fit" rotation was clockwise around a vertical axis for the Glen River locality and anti-clockwise for the Bloody Bridge River locality (Table 1)—and not a rotation around a horizontal axis, as expected by laccolith inflation. Additionally, the agreement
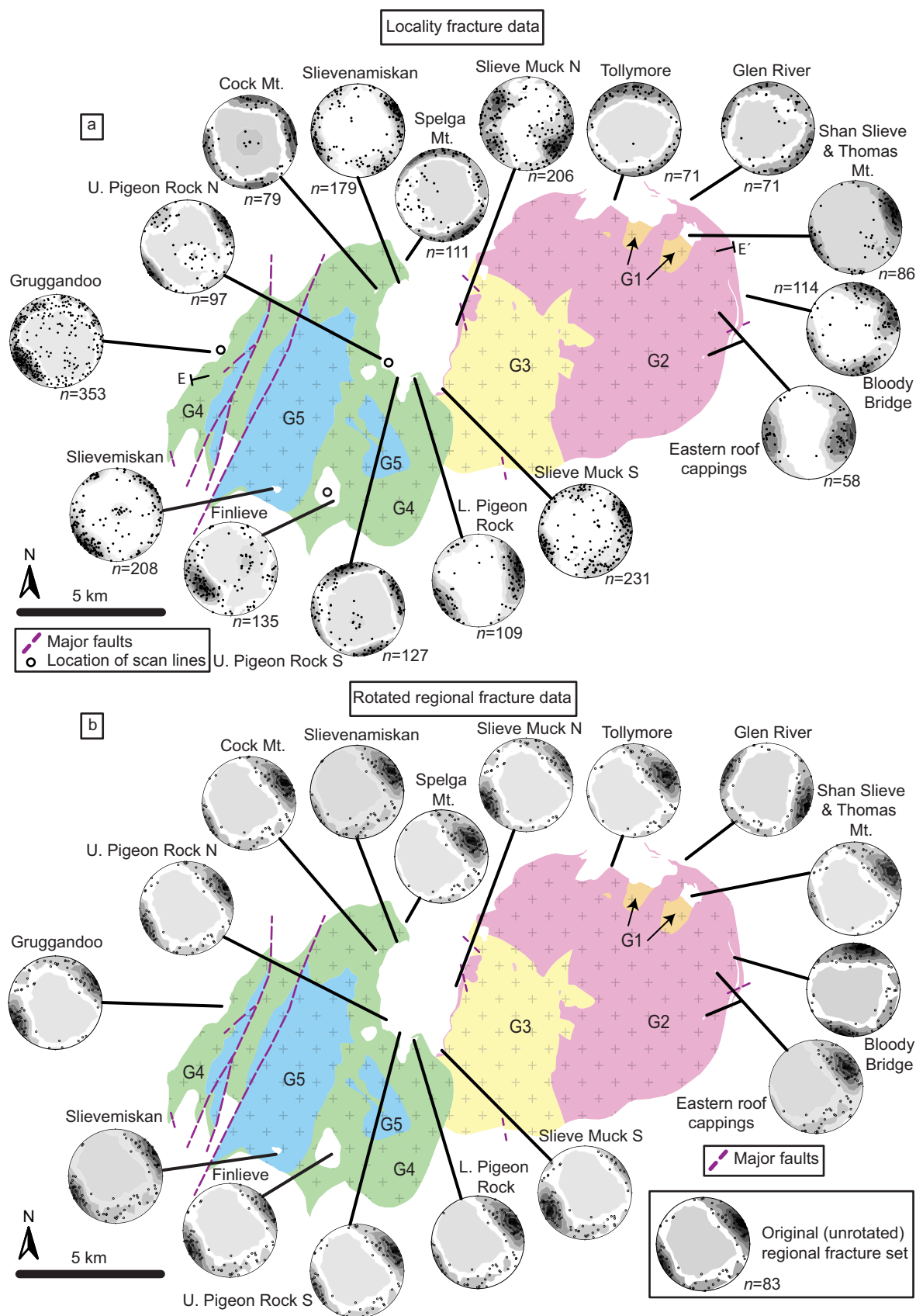
Figure 12. Comparative figure between the fracture data measured in situ in the field (A) and regional fracture data rotated to reflect laccolith inflation (B). If the host rock had been rotated by laccolith inflation, the rotated fracture pattern in (B) should largely reflect the host-rock fracture pattern at the respective locality shown in (A). Details are given below. (A) Poles to fracture planes measured in situ at the fracture-study localities plotted in lower-hemisphere contoured Schmidt stereonets. E and E′ indicate the location of cross section in Figure 13. (B) Poles to regional fracture planes plotted in lower-hemisphere contoured Schmidt stereonets rotated according to the Mourne pluton roof orientation at each fracture-study locality. Only steeply dipping fractures were rotated because the data density for shallow dipping fractures are too sparse for a reliable comparison of fracture orientations between measurement localities (cf. Fig. 10A).The fracture-study localities are shown on the map of the Mourne granite pluton (redrawn after Hood, 1981 and Gibson, 1984). The stereonets were contoured with Kamb contouring with a contour interval of 2σ and a significance level of 3σ. See Table 1 for the degree and orientation of rotation (strike and dip of contact at locality). See also Supplemental Figure S5 (text footnote 1), where the rotation expected from laccolith inflation has been subtracted from the respective host-rock locality fracture data seen in (A) and should therefore reflect the host-rock fracture orientations before laccolith inflation, on the condition that laccolith inflation has occurred.

between the rotated regional fractures and the in situ–measured fracture sets in the wall outcrops suggests that the regional fracture sets in the roof exposures would indeed also have been rotated if laccolith inflation had occurred. See Table 1 for degree of rotation; Figure 12 and Supplemental Table S5 for comparison between the in situ–measured fracture data and the rotated regional fracture set; and Supplemental Figure S4 (footnote 1) for the contact orientation subtracted from the in situ–measured fracture data at each locality (see above for details).

5.4. Deformation in the Contact-Metamorphic Aureole

The small displacements of the contact-metamorphic segregations along fractures in several of the samples show that contact-metamorphic alteration occurred partly before deformation in the aureole (Figs. 6C and 6D). This deformation was likely associated with the emplacement of the Mourne granites, since several fractures are filled with contact-metamorphic minerals (see Table S1). Numerical models indicate that several thousands of years are required for host rock located ~1 km from the intrusion to reach peak contact-metamorphic conditions (cf. Cui et al., 2003; Douglas et al., 2016). Notably, the emplacement-related deformation is primarily observed in the distal samples (relative to the granite) of the Glen River traverse (samples GRT-10–15). This deformation pattern suggests that initial emplacement of magma in the Mourne granite pluton did not cause significant deformation of the roof and wall of the pluton, while later granite emplacement is associated with deformation. The aureole to the Eastern Mourne pluton therefore records different stages of emplacement of the granite. A pattern of initial alteration followed by deformation has also been documented in aureoles to other plutons (see Morgan et al., 1998; Morgan, 2018). The deformed contact-metamorphic segregations in the host rock could reflect different laccolith growth stages, where the initial sill emplacement is accommodated by elastic deformation of the host rock (e.g., Pollard and Johnson, 1973; Jackson and Pollard, 1990; Bunger and Cruden, 2011; Michaut, 2011). The deformation of the segregations would then record the inflation of a sill to a laccolith (cf. de Saint-Blanquat et al., 2006). However, the existence of fractures, faults, and folds associated with the growth of sills and stacked-sill–type laccoliths (Pollard et al., 1975; de Saint-Blanquat et al., 2006; Schofield et al., 2012; Schmiedel et al., 2015; Wilson et al., 2016; Spacapan et al., 2017; Galland et al., 2019) have led some authors to question the role of elastic deformation during sill and laccolith emplacement (Haug et al., 2017; Scheibert et al., 2017).

The brecciated contact-metamorphic segregations and cataclasite in the Glen River and Bloody Bridge River traverses show that granite emplacement was associated with significant deformation on the northeastern wall of the pluton (Figs. 6A–6D; Table S1 [footnote 1]). Stevenson et al. (2007) noted a pluton-side-up sense of shear in cataclasite in G2 on Millstone Mountain located ~1 km NNW of the sedimentary screen. Moreover, the brecciation in the distal samples of the Glen River traverse might mark the location of the

transition between deflected host rock and graywacke unaffected by the emplacement of the granites. Our observations in the aureole suggest that neither cauldron subsidence emplacement, which would not cause significant deformation of the roof and wall of the pluton, nor laccolith emplacement, which would likely be associated with deformation throughout granite emplacement, can solely explain the deformation pattern in the aureole.

6. EMPLACING THE MOURNE GRANITES

The conjugate fractures in G1 (Fig. 4F), the rotation of the host rock along the northeastern contact (Figs. 2A and 12), the displaced contact-metamorphic segregations (Fig. 6), and potential uplift and rotation of the roof along the southwestern border of the intrusion point to intrusive deformation of the host during the emplacement of the granites. These observations do not support cauldron subsidence as a mechanism of emplacement; however, the host-rock deformation pattern to the Mourne granite pluton is also largely inconsistent with the expected deformation caused by a laccolith emplaced along a horizontal floor. For example, the regional fracture pattern can be reconstructed by rotation around a vertical axis (as opposed to a horizontal axis) in the wall rock to the Mourne granite pluton in the NE, while the nearby roof exposures (Thomas Mountain and Tollymore) show no distinct rotation (Fig. 12). The reported subhorizontal magnetic fabrics in the interior of the Mourne pluton and the shallowly inclined fabrics close to the contact indicate a largely contact-parallel, magnetic-fabric geometry (Stevenson et al., 2007; Stevenson and Bennett, 2011). The lack of studies of the magmatic fabric in plutons emplaced by floor subsidence makes it hard to pinpoint magma flow patterns related to floor subsidence. Moreover, in plutons, where the magmatic fabric does not record the regional strain, the fabric is commonly parallel to the contact with host rock (Buddington, 1959; Bateman et al., 1963; Paterson and Tobisch, 1988; Paterson et al., 1998). A contact-parallel magmatic fabric is therefore not sufficient evidence of laccolith inflation. The different local responses of the host rock to the emplacement of the granite pluton are hence held to either reflect laccolith (western part of the pluton) and bysmalith (eastern part of pluton) emplacement along a curved floor or multiple mechanisms of emplacement, both floor subsidence and roof uplift and wall deflection.

Magma emplacement through inflation of an inclined and curved (convex) sill and associated uplift of the roof along faults would result in a dome-shaped roof to the pluton. However, sill geometries are usually flat or saucer-shaped (flat base with upwardly inclined sheets; Galland et al., 2018), irrespective of the orientation of host-rock discontinuities (cf. Stephens et al., 2017). Moreover, laccoliths have been suggested to become less common at intrusion depths of more than three kilometers in favor of sills and lopoliths (Corry, 1988; Roman-Berdiel et al., 1995; Cruden, 1998; Cruden and McCaffrey, 2001). The floor to the Mourne pluton was likely located below three kilometers depth for most of the duration of emplacement (see section 2.3.). We therefore deem the inflation of a dome-shaped sill an unlikely emplacement mechanism of the

Mourne granite pluton. The southwestern succession of the Mourne granites (G1 to G4) and the shallow northeastward dip of the internal contacts in the Eastern Mourne pluton and granite-graywacke contact in the eastern part of the Western Mourne pluton thus suggest asymmetric floor subsidence. This implies that the area of maximum subsidence is not located in the center of the subsiding floor (Lipman, 1984). The slightly dome-shaped roof of the pluton could therefore be attributed to the bell-jar geometry of the subsidence-related faults that generally form during cauldron subsidence or caldera collapse (Anderson, 1937; Holohan et al., 2015).

A possible mechanism responsible for the deflection of the wall rock parallel to the strike of the contact is viscous indentation of the wall rock during expansion of the pluton (cf. Merle and Donnadieu, 2000; Mathieu et al., 2008; Spacapan et al., 2017; Galland et al., 2018). However, floor subsidence may

also have induced shear parallel to the strike of the contact (Fig. 13). Holohan et al. (2013) showed that asymmetric floor subsidence could produce oblique-slip caldera faults. Asymmetric floor subsidence could also explain the opposite rotations inferred (from the rotation model) at the wall-rock localities assuming the area of maximum subsidence is located between the Glen and Bloody Bridge Rivers (Fig. 2A; Table 1), although we lack field observations from the wall-rock outcrops that indicate the sense of shear.

The dike-like tips of the semi-circular northeastern contact could represent part of the feeder to the pluton (Richey, 1927; Walker, 1975; Hood, 1981). The dominantly shallow dips of the magnetic fabric in the area led Stevenson et al. (2007) to favor a feeder in the SW, while they also considered a feeder in the NE a possibility. Since the current exposures of the granite in the northeastern part of the pluton were likely located close to the roof (Fig. 5). The magnetic
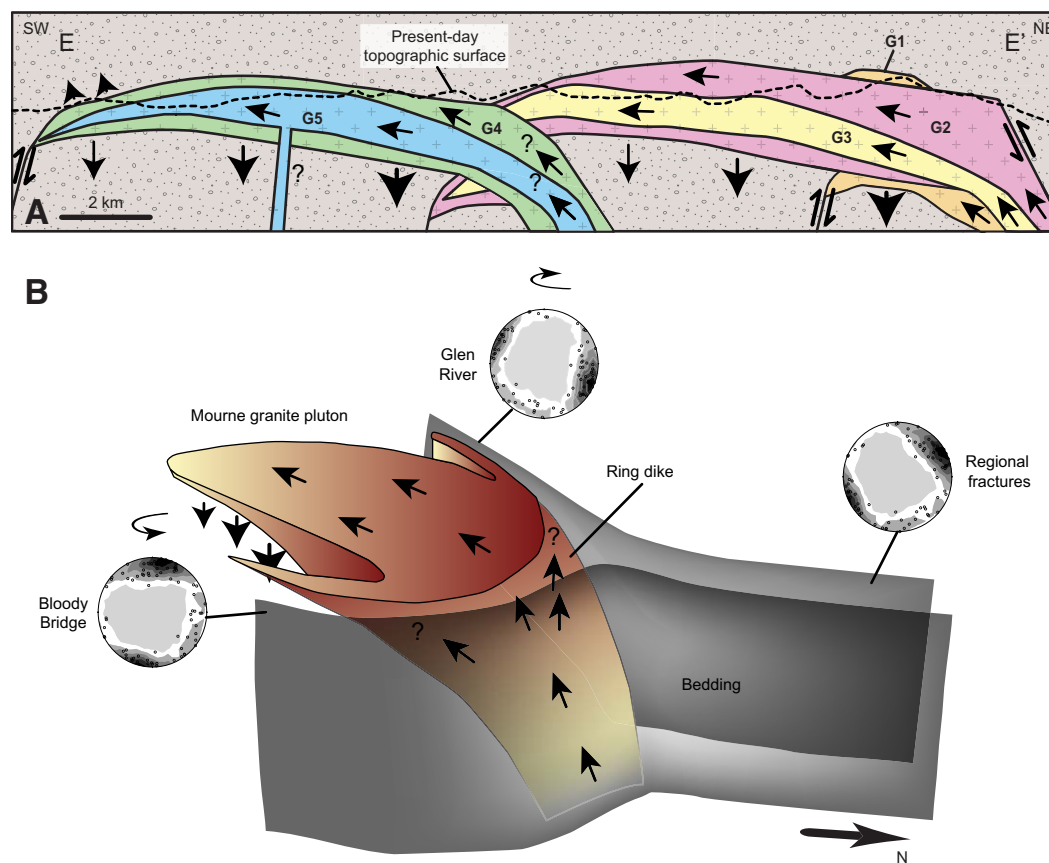

Figure 13. (A) Schematic cross section of the floor-subsidence emplacement model for the Mourne granite pluton. The location of section E–E' is given in Figure 12A. The semi-circular northeastern contact to the pluton and the recorded deformation in the host rock in the NE suggest that the granites G1–G3 were fed from a ring dike and flowed laterally toward the SW (cf. Stevenson et al., 2007). The Western Mourne pluton granites could have been fed from the same direction. Alternatively, G4 and G5 could have been fed from a central feeder. The smaller black arrows indicate magma flow, and the larger arrows show the displacement of the host rock. The pluton floor is not exposed in the Mourne Mountains; therefore, the pluton may be thicker. (B) Schematic sketch of granite emplacement along the northeastern contact of the Mourne granite pluton. The observed rotation of the host rock and the regional fractures at the northeastern contact are proposed to be caused by contact-parallel shear due to asymmetric floor subsidence or viscous indentation of the wall close to the feeder of the pluton. The rotation of the wall rock is indicated by the stereonets, which show the rotated regional fracture sets of the Bloody Bridge and Glen River localities (cf. Fig. 12B).

mineral fabric may therefore record compaction or imbrication of magma as a result of the shear between the magma and the host rock (cf. Knight and Walker, 1988; Geoffroy et al., 2002; Eriksson et al., 2011; Mattsson et al., 2018). We therefore agree with previously presented magma emplacement models (Richey, 1927; Walker, 1975; Hood, 1981; Stevenson et al., 2007), which suggest that the Eastern Mourne granitic magma was fed from the NE and then spread laterally toward the west and SW.

The Western Mourne granite pluton was suggested to be fed from a magma body in the Carlingford Lough with the magma inlet located at the SSW margin of the pluton, based on a NNE-SSW trend of a subhorizontal magnetic lineation in the center of the pluton (Stevenson and Bennett, 2011). The cone sheets surrounding, and pre-dating, the Mourne granite pluton point to the existence of a mafic source magma chamber located below the granites (Emeleus, 1955; Akiman, 1971; Hood, 1981). Such a mafic body could explain the absence of a negative gravity anomaly in the area of the Mourne granite pluton, because the positive gravity anomaly associated with such a mafic pluton could cancel out the common negative gravity signal caused by a granite (Bean, 1953; Bott, 1956; Bott et al., 1958). Notably, the nearby Newry granites show a negative gravity anomaly (cf. Reay, 2004; Stevenson and Bennett, 2011). A mafic source magma body is also consistent with petrological data that indicate that the Mourne granites formed by differentiation from a basaltic magma (Meighan et al., 1984). We therefore propose two possible feeder locations to the Western Mourne pluton. The gently inclined contacts to the E-NE in the eastern part of the Western Mourne pluton indicate floor geometry similar to the Eastern Mourne pluton and together with the observed doming in the west suggest a magma flow from the NE. Alternatively, the NNE-SSW magnetic lineation could indicate a central feeder (Fig. 13).

■ 7. CONCLUSIONS

In this study, we investigated the host-rock deformation related to the emplacement of the Paleogene Mourne granites by using the fracture pattern in the host rock. The fractures in the granite host rock dip steeply and cluster in four major sets striking SE, S, NE, and E. The most dominant fracture sets that strike toward the SE and NE correlate with the regional fracture sets that formed during the Caledonian orogeny. Since rotation of the pluton roof caused by laccolith inflation would have largely shallowed the inclination of the regional fracture sets, the consistently steep dip of the regional fractures in the roof rock does not support significant rotation of the roof, especially where the dip of the contact is ~20°. However, the wall rock at the northeastern contact to the pluton shows steeply inclined fractures with diverging fracture strikes compared to the regional fracture sets. We propose that their orientations reflect rotation of the wall parallel to the strike of the contact to the Mourne granite pluton.

Several contact-metamorphic segregations in the aureole to the Mourne granites show small displacements (≤1 mm) along fractures. This suggests that the initial emplacement of magma in the Mourne granite pluton caused contact metamorphism but did not cause significant deformation, while later granite emplacement is associated with deformation. Additionally, the displaced and brecciated contact-metamorphic segregations and the occurrence of cataclasite and breccia in the Glen River and Bloody Bridge River traverses indicate that granite emplacement was associated with significant deformation on the northeastern wall of the pluton. The aureole therefore records multiple growth stages of the pluton or different granite pulses emplaced in slightly different fashions.

The lack of pluton-wide rotational deformation in the roof to the granite pluton, the westward younging succession of the granites, and granite-granite contacts inclined toward the NE in the Eastern Mourne pluton suggest that granite emplacement was either (1) facilitated by trap-door floor subsidence combined with local roof uplift in the SW and wall deflection during a later stage of emplacement; or (2) as laccoliths and bysmaliths with a curved floor, which explain the lack of distinct rotation of the roof. The bulk of the uplift would then have been facilitated by a fault. However, we favor the first scenario, because a curved (convex) sill geometry as required for the second emplacement scenario is not commonly observed in nature (see section 6). Furthermore, we suggest that the rotation of the wall rock parallel to the strike of the contact to the pluton, as inferred by the rotation model, was related to asymmetric floor subsidence and/or viscous indentation of the wall rock.

REFERENCES CITED

Akiman, O., 1971, The petrology and geochemistry of the tertiary dyke swarm associated with the Mourne Mountain granites, Northern Ireland [Ph.D. dissertation]: University of Durham, Durham, 131 p.

Allen, P.A., et al., 2002, The post-Variscan thermal and denudational history of Ireland, *in* Doré, A.G., Cartwright, J.A., Stoker, M.S., Turner, J.P., and White, N., eds., Exhumation of the North Atlantic Margin: Timing, Mechanisms and Implications for Petroleum Exploration: Geological Society of London Special Publication 196, p. 371–399, https://doi.org/10.1144/GSL.SP.2002.196.01.20.

Allmendinger, R.W., Cardozo, N., and Fisher, D., 2012, Structural Geology Algorithms: Vectors and Tensors: Cambridge, Cambridge University Press, 289 p.

Allmendinger, R.W., Siron, C.R., and Scott, C.P., 2017, Structural data collection with mobile devices: Accuracy, redundancy, and best practices: Journal of Structural Geology, v. 102, p. 98–112, https://doi.org/10.1016/j.jsg.2017.07.011.

Anderson, E.M., 1937, IX.—The Dynamics of the Formation of Cone-Sheets, Ring-Dykes, and Caldron-Subsidences: Proceedings of the Royal Society of Edinburgh, v. 56, p. 128–157, https://doi.org/10.1017/S0370164600014954.

Anderson, T.B., 1987, The onset and timing of Caledonian sinistral shear in County Down: Journal of the Geological Society of London, v. 144, p. 817–825, https://doi.org/10.1144/gsjgs.144.5.0817.

Anderson, T.B., 2000, Structural interpretations of the Southern Uplands Terrane: Transactions of the Royal Society of Edinburgh. Earth Sciences, v. 91, p. 363–373, https://doi.org/10.1017/S0263593300008245.

Anderson, T.B., 2004, Southern Uplands-Down-Longford Terrane, in Mitchell, W.I., ed., The Geology of Northern Ireland: Our Natural Foundation: Belfast, Geological Survey of Northern Ireland, p. 41–60.

Anderson, T.B., and Cameron, T.D.J., 1979, A structural profile of Caledonian deformation in Down, in Harris, A.L., Holland, C.H., and Leake, B.E., eds., The Caledonides of the British Isles—Reviewed: Geological Society of London Special Publication 8, p. 263–267, https://doi.org/10.1144/GSL.SP.1979.008.01.27.

Bateman, P.C., Clark, L.D., Huber, N.K., Moore, J.G., and Rinehart, C.D., 1963, The Sierra Nevada batholith—A synthesis of recent work across the central part: U.S. Geological Survey Professional Paper 414-D, 46 p., https://doi.org/10.3133/pp414D.

Beamish, D., Kimbell, G.S., Stone, P., and Anderson, T.B., 2010, Regional conductivity data used to reassess Early Palaeozoic structure in the Northern Ireland sector of the Southern Uplands–Down-Longford terrane: Journal of the Geological Society of London, v. 167, no. 4, p. 649–657, https://doi.org/10.1144/0016-76492009-122.

Bean, R.J., 1953, Relation of gravity anomalies to the geology of central Vermont and New Hampshire: Geological Society of America Bulletin, v. 64, p. 509–538, https://doi.org/10.1130/0016-7606(1953)64[509:ROGATT]2.0.CO;2.

Bergbauer, S., and Martel, S.J., 1999, Formation of joints in cooling plutons: Journal of Structural Geology, v. 21, p. 821–835, https://doi.org/10.1016/S0191-8141(99)00082-6.

Bott, M.H.P., 1956, A geophysical study of the granite problem: Quarterly Journal of the Geological Society of London, v. 112, p. 45–67, https://doi.org/10.1144/GSL.JGS.1956.112.01-04.04.

Bott, M.H.P., Day, A.A., and Masson-Smith, D., 1958, The geological interpretation of gravity and magnetic surveys in Devon and Cornwall: Philosophical Transactions of the Royal Society A: Mathematical, Physical and Engineering Sciences, v. 251, p. 161–191, https://doi.org/10.1098/rsta.1958.0013.

Bowen, N.L., 1948, The granite problem and the method of multiple prejudices, in Gilluly, J., Read, H.H., Buddington, A.F., Grout, F.F., Goodspeed, G.E., and Bowen, N.L., eds., Origin of Granite: Geological Society of America Memoir 28, p. 79–90, https://doi.org/10.1130/MEM28-p79.

Branney, M., and Acocella, V., 2015, Calderas, in Sigurdsson, H., ed., The Encyclopedia of Volcanoes: Elsevier, p. 299–315, https://doi.org/10.1016/B978-0-12-385938-9.00016-X.

Buckley, S.J., Ringdal, K., Naumann, N., Dolva, B., Kurz, T.H., Howell, J.A., and Dewez, T.J.B., 2019, LIME: Software for 3-D visualization, interpretation, and communication of virtual geoscience models: Geosphere, v. 15, p. 222–235, https://doi.org/10.1130/GES02002.1.

Buddington, A., 1959, Granite emplacement with special reference to North America: Geological Society of America Bulletin, v. 70, p. 671–747, https://doi.org/10.1130/0016-7606(1959)70[671:GEWSRT]2.0.CO;2.

Bunger, A.P., and Cruden, A.R., 2011, Modeling the growth of laccoliths and large mafic sills: Role of magma body forces: Journal of Geophysical Research, v. 116, B02203, https://doi.org/10.1029/2010JB007648.

Burchardt, S., 2018, Introduction to volcanic and igneous plumbing systems—Developing a discipline and common concepts, in Burchardt, S., ed., Volcanic and Igneous Plumbing Systems: Amsterdam, Elsevier, p. 1–12, https://doi.org/10.1016/B978-0-12-809749-6.00001-7.

Burchardt, S., Tanner, D.C., and Krumbholz, M., 2010, Mode of emplacement of the Slaufrudalur Pluton, Southeast Iceland inferred from three-dimensional GPS mapping and model building: Tectonophysics, v. 480, p. 232–240, https://doi.org/10.1016/j.tecto.2009.10.010.

Burchardt, S., Tanner, D., and Krumbholz, M., 2012, The Slaufrudalur pluton, southeast Iceland—An example of shallow magma emplacement by coupled cauldron subsidence and magmatic stoping: Geological Society of America Bulletin, v. 124, p. 213–227, https://doi.org/10.1130/B30430.1.

Burchardt, S., Troll, V.R., Mathieu, L., Emeleus, H.C., and Donaldson, C.H., 2013, Ardnamurchan 3D cone-sheet architecture explained by a single elongate magma chamber: Scientific Reports, v. 3, p. 2891, https://doi.org/10.1038/srep02891.

Cloos, H., 1922, Tektonik und Magma: Untersuchungen zur Geologie der Tiefe: Band 1, Abhandlungen des Preussischen Geologischen Landesanstalt, v. 89, 142 p.

Clough, C.T., Maufe, H.B., and Bailey, E.B., 1909, The Cauldron-Subsidence of Glen Coe, and the Associated Igneous Phenomena: Quarterly Journal of the Geological Society of London, v. 65, p. 611–678, https://doi.org/10.1144/GSL.JGS.1909.065.01-04.35.

Cooper, M.R., 2004, Palaeogene Extrusive Igneous Rocks, in Mitchell, W.I., ed., The Geology of Northern Ireland: Our Natural Foundation: Belfast, Geological Survey of Northern Ireland, p. 167–178.

Cooper, M.R., and Johnston, T.P., 2004, Palaeogene Intrusive Igneous Rocks, in Mitchell, W.I. ed., The Geology of Northern Ireland: Belfast, Our Natural Foundation, Geological Survey of Northern Ireland, p. 179–198.

Cooper, M.R., Anderson, H., Walsh, J.J., Van Dam, C.L., Young, M.E., Earls, G., and Walker, A., 2012, Palaeogene Alpine tectonics and Icelandic plume-related magmatism and deformation in Northern Ireland: Journal of the Geological Society of London, v. 169, p. 29–36, https://doi.org/10.1144/0016-76492010-182.

Corry, C.E., 1988, Laccoliths; Mechanics of Emplacement and Growth: Geological Society of America Special Paper 220, p. 1–114, https://doi.org/10.1130/SPE220-p1.

Cruden, A.R., 1998, On the emplacement of tabular granites: Journal of the Geological Society of London, v. 155, p. 853–862, https://doi.org/10.1144/gsjgs.155.5.0853.

Cruden, A.R., and McCaffrey, K.J.W., 2001, Growth of plutons by floor subsidence: Implications for rates of emplacement, intrusion spacing and melt-extraction mechanisms: Physics and Chemistry of the Earth. Part A: Solid Earth and Geodesy, v. 26, p. 303–315, https://doi.org/10.1016/S1464-1895(01)00060-6.

Cui, X., Nabelek, P.I., and Liu, M., 2003, Reactive flow of mixed CO_2-H_2O fluid and progress of calc-silicate reactions in contact metamorphic aureoles: Insights from two-dimensional numerical modelling: Journal of Metamorphic Geology, v. 21, p. 663–684, https://doi.org/10.1046/j.1525-1314.2003.00475.x.

Daly, R.A., 1903, The mechanics of igneous intrusion: American Journal of Science, v. 15, p. 269–298, https://doi.org/10.2475/ajs.s4-15.88.269.

de Saint-Blanquat, M., Habert, G., Horsman, E., Morgan, S.S., Tikoff, B., Launeau, P., and Gleizes, G., 2006, Mechanisms and duration of non-tectonically assisted magma emplacement in the upper crust: The Black Mesa pluton, Henry Mountains, Utah: Tectonophysics, v. 428, p. 1–31, https://doi.org/10.1016/j.tecto.2006.07.014.

Douglas, M.M., Geyer, A., Álvarez-Valero, A.M., and Martí, J., 2016, Modeling magmatic accumulations in the upper crust: Metamorphic implications for the country rock: Journal of Volcanology and Geothermal Research, v. 319, p. 78–92, https://doi.org/10.1016/j.jvolgeores.2016.03.008.

Emeleus, C.H., 1955, The granites of the western Mourne Mountains, County Down: The Scientific Proceedings of the Royal Dublin Society: Royal Dublin Society, v. 27, p. 35–52.

Emeleus, C.H., and Bell, B.R., 2005, British Regional Geology: The Palaeogene Volcanic Districts of Scotland: Nottingham, British Geological Survey, 214 p.

Emeleus, C.H., and Preston, J., 1969, Field excursion guide to the Tertiary volcanic rocks of Ireland, in Francis, E.H., ed., Oxford, International Association of Volcanology and Chemistry of the Earth's Interior Symposium, 71 p.

Eriksson, P.I., Riishuus, M.S., Sigmundsson, F., and Elming, S.-Å., 2011, Magma flow directions inferred from field evidence and magnetic fabric studies of the Streitishvarf composite dike in east Iceland: Journal of Volcanology and Geothermal Research, v. 206, p. 30–45, https://doi.org/10.1016/j.jvolgeores.2011.05.009.

Feng, Z., Wang, C., Liang, J., Li, J., Huang, Y., Liao, J., and Wang, R., 2011, The emplacement mechanisms and growth styles of the Guposhan-Huashan batholith in western Nanling Range, South China: Science China. Earth Sciences, v. 54, p. 45–60, https://doi.org/10.1007/s11430-010-4143-4.

Fisher, N.I., Lewis, T., and Embleton, B.J.J., 1993, Statistical Analysis of Spherical Data: Cambridge, UK, Cambridge University Press, 343 p.

Fossen, H., 2010, Structural Geology: Cambridge, UK, Cambridge University Press, 463 p., https://doi.org/10.1017/CBO9780511777806.

Galland, O., Bertelsen, H.S., Eide, C.H., Guldstrand, F, Haug, Ø.T., Leanza, H.A., Mair, K., Palma, O., Planke, S., Rabbel, O., Rogers, B., Schmiedel, T., Souche, A., and Spacapan, J.B., 2018, Storage and Transport of Magma in the Layered Crust—Formation of Sills and Related Flat-Lying Intrusions, in Burchardt, S., ed., Volcanic and Igneous Plumbing Systems: Elsevier, p. 113–138, https://doi.org/10.1016/B978-0-12-809749-6.00005-4.

Galland, O., Spacapan, J.B., Rabbel, O., Mair, K., Soto, F.G., Eiken, T., Schiuma, M., and Leanza, H.A., 2019, Structure, emplacement mechanism and magma-flow significance of igneous

fingers—Implications for sill emplacement in sedimentary basins: Journal of Structural Geology, v. 124, p. 120–135, https://doi.org/10.1016/j.jsg.2019.04.013.

Gamble, J.A., Wysoczanski, R.J., and Meighan, I.G., 1999, Constraints on the age of the British Tertiary Volcanic Province from ion microprobe U-Pb (SHRIMP) ages for acid igneous rocks from NE Ireland: Journal of the Geological Society of London, v. 156, p. 291–299, https://doi.org/10.1144/gsjgs.156.2.0291.

Ganerød, M., Smethurst, M.A., Torsvik, T.H., Prestvik, T., Rousse, S., McKenna, C., Van Hinsbergen, D.J.J., and Hendriks, B.W.H., 2010, The North Atlantic Igneous Province reconstructed and its relation to the Plume Generation Zone: The Antrim Lava Group revisited: Geophysical Journal International, v. 182, p. 183–202, https://doi.org/10.1111/j.1365-246X.2010.04620.x.

Geoffroy, L., Callot, J.P., Aubourg, C., and Moreira, M., 2002, Magnetic and plagioclase linear fabric discrepancy in dykes: A new way to define the flow vector using magnetic foliation: Terra Nova, v. 14, p. 183–190, https://doi.org/10.1046/j.1365-3121.2002.00412.x.

Gibson, D., 1984, The petrology and geochemistry of the Western Mourne granites, Co. Down, N Ireland [Ph.D. dissertation]: Belfast, Queen's University, 351 p.

Gibson, D., McCormick, A.G., Meighan, I.G., and Halliday, A.N., 1987, The British Tertiary Igneous Province: Young Rb-Sr Ages for the Mourne Mountains Granites: Scottish Journal of Geology, v. 23, p. 221–225, https://doi.org/10.1144/sjg23020221.

Gibson, D., Lux, D.R., and Meighan, I.G., 1995, New $^{40}Ar/^{39}Ar$ Ages for the Mourne Mountains Granites, North-East Ireland: Israel Journal of Earth Sciences, v. 14, p. 25–35.

Gilbert, G.K., 1877, Report on the geology of the Henry Mountains: Washington, D.C., U.S. Geographical and Geological Survey, 160 p.

Haug, Ø.T., Galland, O., Souloumiac, P., Souche, A., Guldstrand, F., and Schmiedel, T., 2017, Inelastic damage as a mechanical precursor for the emplacement of saucer-shaped intrusions: Geology, v. 45, p. 1099–1102, https://doi.org/10.1130/G39361.1.

Hawkes, L., and Hawkes, H.K., 1933, The Sandfell Laccolith and 'Dome of Elevation': Quarterly Journal of the Geological Society of London, v. 89, p. 379–400, https://doi.org/10.1144/GSL.JGS.1933.089.01-04.14.

Holohan, E.P., Troll, V.R., Walter, T.R., Münn, S., McDonnell, S., and Shipton, Z.K., 2005, Elliptical calderas in active tectonic settings: An experimental approach: Journal of Volcanology and Geothermal Research, v. 144, p. 119–136, https://doi.org/10.1016/j.jvolgeores.2004.11.020.

Holohan, E.P., Walter, T.R., Schöpfer, M.P.J., Walsh, J.J., van Wyk de Vries, B., and Troll, V.R., 2013, Origins of oblique-slip faulting during caldera subsidence: Journal of Geophysical Research. Solid Earth, v. 118, p. 1778–1794, https://doi.org/10.1002/jgrb.50057.

Holohan, E.P., Schöpfer, M.P.J., and Walsh, J.J., 2015, Stress evolution during caldera collapse: Earth and Planetary Science Letters, v. 421, p. 139–151, https://doi.org/10.1016/j.epsl.2015.03.003.

Hood, D.N., 1981, Geochemical, petrological and structural studies on the tertiary granites and associated rocks of the Eastern Mourne Mountains, Co. Down, Northern Ireland [M.S. thesis]: Belfast, Queen's University, 520 p.

Hutton, D.H.W., 1988, Granite emplacement mechanisms and tectonic controls: Inferences from deformation studies: Transactions of the Royal Society of Edinburgh. Earth Sciences, v. 79, p. 245–255, https://doi.org/10.1017/S0263593300014255.

Hutton, D.H.W., Dempster, T.J., Brown, P.E., and Becker, S.D., 1990, A new mechanism of granite emplacement: Intrusion in active extensional shear zones: Nature, v. 343, p. 452–455, https://doi.org/10.1038/343452a0.

Jackson, M.D., and Pollard, D.D., 1990, Flexure and faulting of sedimentary host rocks during growth of igneous domes, Henry Mountains, Utah: Journal of Structural Geology, v. 12, p. 185–206, https://doi.org/10.1016/0191-8141(90)90004-I.

Johnson, A.M., and Pollard, D.D., 1973, Mechanics of growth of some laccolithic intrusions in the Henry Mountains, Utah, I: Tectonophysics, v. 18, p. 261–309, https://doi.org/10.1016/0040-1951(73)90050-4.

Johnston, T.P., 2004, Post-Variscan Deformation and Basin Formation, in Mitchell, W.I., ed., The geology of Northern Ireland: Our Natural Foundation: Belfast, Geological Survey of Northern Ireland, p. 205–210.

Kennedy, B., Wilcock, J., and Stix, J., 2012, Caldera resurgence during magma replenishment and rejuvenation at Valles and Lake City calderas: Bulletin of Volcanology, v. 74, p. 1833–1847, https://doi.org/10.1007/s00445-012-0641-x.

Kennedy, B.M., Holohan, E.P., Stix, J., Gravley, D., Davidson, J.P., Cole, J., and Burchardt, S., 2018, Volcanic and Igneous Plumbing Systems of Caldera Volcanoes, in Burchardt, S., ed., Volcanic and Igneous Plumbing Systems: Amsterdam, Elsevier, p. 259–284, https://doi.org/10.1016/B978-0-12-809749-6.00010-8.

Knight, M.D., and Walker, G.P.L., 1988, Magma flow directions in dikes of the Koolau Complex, Oahu, determined from magnetic fabric studies: Journal of Geophysical Research, v. 93, p. 4301, https://doi.org/10.1029/JB093iB05p04301.

Lato, M.J., Diederichs, M.S., and Hutchinson, D.J., 2010, Bias correction for view-limited lidar scanning of rock outcrops for structural characterization: Rock Mechanics and Rock Engineering, v. 43, p. 615–628, https://doi.org/10.1007/s00603-010-0086-5.

Lawver, L.A., and Muller, R.D., 1994, Iceland hotspot track: Geology, v. 22, p. 311–314, https://doi.org/10.1130/0091-7613(1994)022<0311:IHT>2.3.CO;2.

Lipman, P.W., 1984, The roots of ash flow calderas in western North America: Windows into the tops of granitic batholiths: Journal of Geophysical Research, v. 89, p. 8801, https://doi.org/10.1029/JB089iB10p08801.

Mardia, K.V., 1975, Statistics of Directional Data: Journal of the Royal Statistical Society. Series B. Methodological, v. 37, p. 349–393.

Mathieu, L., van Wyk de Vries, B., Holohan, E.P., and Troll, V.R., 2008, Dykes, cups, saucers and sills: Analogue experiments on magma intrusion into brittle rocks: Earth and Planetary Science Letters, v. 271, p. 1–13, https://doi.org/10.1016/j.epsl.2008.02.020.

Mattsson, T., Burchardt, S., Almqvist, B.S.G., and Ronchin, E., 2018, Syn-emplacement fracturing in the Sandfell Laccolith, eastern Iceland—Implications for rhyolite intrusion growth and volcanic hazards: Frontiers of Earth Science, v. 6, p. 5, https://doi.org/10.3389/feart.2018.00005.

Meighan, I.G., Gibson, D., and Hood, D.N., 1984, Some aspects of Tertiary acid magmatism in NE Ireland: Mineralogical Magazine, v. 48, p. 351–363, https://doi.org/10.1180/minmag.1984.048.348.05.

Merle, O., and Donnadieu, F., 2000, Indentation of volcanic edifices by the ascending magma, in Vendeville, B.C., Mart, Y., and Vigneresse, J.-L., eds., Salt, Shale and Igneous Diapirs in and around Europe: Geological Society of London Special Publication 174, p. 43–53, https://doi.org/10.1144/GSL.SP.1999.174.01.03.

Merriman, R.J., and Roberts, B., 2001, Low-grade metamorphism in the Scottish Southern Uplands Terrane: Deciphering the patterns of accretionary burial, shearing and cryptic aureoles: Transactions of the Royal Society of Edinburgh. Earth Sciences, v. 91, Part 3, p. 521–537, https://doi.org/10.1017/S0263593300008373.

Michaut, C., 2011, Dynamics of magmatic intrusions in the upper crust: Theory and applications to laccoliths on Earth and the Moon: Journal of Geophysical Research, v. 116, B05205, https://doi.org/10.1029/2010JB008108.

Morgan, S., 2018, Pascal's Principle, a Simple Model to Explain the Emplacement of Laccoliths and Some Mid-crustal Plutons, in Burchardt, S., ed., Volcanic and Igneous Plumbing Systems: Amsterdam, Elsevier, p. 139–165, https://doi.org/10.1016/B978-0-12-809749-6.00006-6.

Morgan, S., Stanik, A., Horsman, E., Tikoff, B., de Saint-Blanquat, M., and Habert, G., 2008, Emplacement of multiple magma sheets and wall rock deformation: Trachyte Mesa intrusion, Henry Mountains, Utah: Journal of Structural Geology, v. 30, p. 491–512, https://doi.org/10.1016/j.jsg.2008.01.005.

Morgan, S.S., Law, R.D., and Nyman, M.W., 1998, Laccolith-like emplacement model for the Papoose Flat pluton based on porphyroblast-matrix analysis: Geological Society of America Bulletin, v. 110, p. 96–110, https://doi.org/10.1130/0016-7606(1998)110<0096:LLEMFT>2.3.CO;2.

Nelson, C.A., and Sylvester, A.G., 1971, Wall Rock Decarbonation and Forcible Emplacement of Birch Creek Pluton, Southern White Mountains, California: Geological Society of America Bulletin, v. 82, p. 2891–2904, https://doi.org/10.1130/0016-7606(1971)82[2891:WRDAFE]2.0.CO;2.

Oliver, G.J.H., and Leggett, J.K., 1980, Metamorphism in an accretionary prism: Prehnite-pumpellyite facies metamorphism of the Southern Uplands of Scotland: Transactions of the Royal Society of Edinburgh. Earth Sciences, v. 71, p. 235–246, https://doi.org/10.1017/S0263593300013602.

Park, H.J., and West, T.R., 2002, Sampling bias of discontinuity orientation caused by linear sampling technique: Engineering Geology, v. 66, p. 99–110, https://doi.org/10.1016/S0013-7952(02)00034-0.

Paterson, S.R., and Fowler, T.K., 1993, Re-examining pluton emplacement processes: Journal of Structural Geology, v. 15, p. 191–206, https://doi.org/10.1016/0191-8141(93)90095-R.

Paterson, S.R., and Tobisch, O.T., 1988, Using pluton ages to date regional deformations: Problems with commonly used criteria: Geology, v. 16, p. 1108, https://doi.org/10.1130/0091-7613(1988)016<1108:UPATDR>2.3.CO;2.

Paterson, S.R., Fowler, T.K., Schmidt, K.L., Yoshinobu, A.S., Yuan, E.S., and Miller, R.B., 1998, Interpreting magmatic fabric patterns in plutons: Lithos, v. 44, p. 53–82, https://doi.org/10.1016/S0024-4937(98)00022-X.

Pattison, D.R.M., and Tracy, R.J., 1991, Phase equilibria and thermobarometry of metapelites, *in* Kerrick, D.M., ed., Reviews in Mineralogy and Geochemistry: Chelsea, Michigan, Mineralogical Society of America, v. 26, p. 105–206.

Petford, N., Cruden, A.R., McCaffrey, K.J.W., and Vigneresse, J.-L., 2000, Granite magma formation, transport and emplacement in the Earth's crust: Nature, v. 408, p. 669–673, https://doi.org/10.1038/35047000.

Pitcher, W.S., 1997, The Nature and Origin of Granite: Dordrecht, Springer Netherlands, 387 p., https://doi.org/10.1007/978-94-011-5832-9.

Pollard, D.D., and Aydin, A., 1988, Progress in understanding jointing over the past century: Geological Society of America Bulletin, v. 100, p. 1181–1204, https://doi.org/10.1130/0016-7606(1988)100<1181:PIUJOT>2.3.CO;2.

Pollard, D.D., and Johnson, A.M., 1973, Mechanics of growth of some laccolithic intrusions in the Henry mountains, Utah, II: Bending and failure of overburden layers and sill formation: Tectonophysics, v. 18, p. 311–354, https://doi.org/10.1016/0040-1951(73)90051-6.

Pollard, D.D., Muller, O.H., and Dockstader, D.R., 1975, The Form and Growth of Fingered Sheet Intrusions: Geological Society of America Bulletin, v. 86, p. 351, https://doi.org/10.1130/0016-7606(1975)86<351:TFAGOF>2.0.CO;2.

Price, N.J., and Cosgrove, J.W., 1990, Analysis of Geological Structures: Cambridge, UK, Cambridge University Press, 502 p.

Quinn, M.F., 2006, Lough Neagh: The site of a Cenozoic pull-apart basin: Scottish Journal of Geology, v. 42, p. 101–112, https://doi.org/10.1144/sjg42020101.

Read, H., 1957, The Granite Controversy: New York, John Wiley & Sons, 430 p.

Reay, D., 2004, Geophysics and concealed geology, *in* Mitchell, W.I., ed., The Geology of Northern Ireland: Our Natural Foundation: Belfast, Geological Survey of Northern Ireland, p. 227–248.

Richards, J.P., 2003, Tectono-Magmatic Precursors for Porphyry Cu-(Mo-Au) Deposit Formation: Economic Geology and the Bulletin of the Society of Economic Geologists, v. 98, p. 1515–1533, https://doi.org/10.2113/gsecongeo.98.8.1515.

Richey, J.E., 1927, The Structural Relations of the Mourne Granites, Northern Ireland: Quarterly Journal of the Geological Society, v. 83, p. 653–689, https://doi.org/10.1144/GSL.JGS.1927.083.01-05.27.

Richey, J.E., Thomas, H.H., Radley, E.G., Dixon, B.E., Eyles, V.A., Lee, G.W., Radley, E.G., and Simpson, J.B., 1930, The Geology of Ardnamurchan, North-West Mull and Coll (A Description of Sheet 51 and Part of Sheet 52 of the Geological Map): Edinburgh, HMSO for the British Geological Survey, v. 51, 393 p.

Robbie, J.A., 1955, The Slieve Binnian tunnel, an aqueduct in the Mourne Mountains: Bulletin of the Geological Survey of Great Britain, v. 8, p. 1–20.

Rohleder, H.P.T., 1931, A Tectonic Analysis of the Mourne Granite Mass, County Down: Proceedings of the Royal Irish Academy. Section B. Biological, Geological and Chemical Science, v. 40, p. 160–174.

Roman-Berdiel, T., Gapais, D., and Brun, J.P., 1995, Analogue models of laccolith formation: Journal of Structural Geology, v. 17, p. 1337–1346, https://doi.org/10.1016/0191-8141(95)00012-3.

Sasvári, Á., and Baharev, A., 2014, SG2PS (structural geology to postscript converter)—A graphical solution for brittle structural data evaluation and paleostress calculation: Computers & Geosciences, v. 66, p. 81–93, https://doi.org/10.1016/j.cageo.2013.12.010.

Scheibert, J., Galland, O., and Hafver, A., 2017, Inelastic deformation during sill and laccolith emplacement: Insights from an analytic elastoplastic model: Journal of Geophysical Research. Solid Earth, v. 122, p. 923–945, https://doi.org/10.1002/2016JB013754.

Schmiedel, T., Breitkreuz, C., Görz, I., and Ehling, B.-C., 2015, Geometry of laccolith margins: 2D and 3D models of the Late Paleozoic Halle Volcanic Complex (Germany): International Journal of Earth Sciences, v. 104, p. 323–333, https://doi.org/10.1007/s00531-014-1085-7.

Schofield, N.J., Brown, D.J., Magee, C., and Stevenson, C.T.E., 2012, Sill morphology and comparison of brittle and non-brittle emplacement mechanisms: Journal of the Geological Society of London, v. 169, p. 127–141, https://doi.org/10.1144/0016-76492011-078.

Scott, C.P., Allmendinger, R.W., González, G., and Loveless, J.P., 2016, Coseismic extension from surface cracks reopened by the 2014 Pisagua, northern Chile, earthquake sequence: Geology, v. 44, p. 387–390, https://doi.org/10.1130/G37662.1.

Senger, K., Buckley, S.J., Chevallier, L., Fagereng, Å., Galland, O., Kurz, T.H., Ogata, K., Planke, S., and Tveranger, J., 2015, Fracturing of doleritic intrusions and associated contact zones: Implications for fluid flow in volcanic basins: Journal of African Earth Sciences, v. 102, p. 70–85, https://doi.org/10.1016/j.jafrearsci.2014.10.019.

Spacapan, J.B., Galland, O., Leanza, H.A., and Planke, S., 2017, Igneous sill and finger emplacement mechanism in shale-dominated formations: A field study at Cuesta del Chihuido, Neuquén Basin, Argentina: Journal of the Geological Society of London, v. 174, p. 422–433, https://doi.org/10.1144/jgs2016-056.

Stephens, T.L., Walker, R.J., Healy, D., Bubeck, A., England, R.W., and McCaffrey, K.J.W., 2017, Igneous sills record far-field and near-field stress interactions during volcano construction: Isle of Mull, Scotland: Earth and Planetary Science Letters, v. 478, p. 159–174, https://doi.org/10.1016/j.epsl.2017.09.003.

Stevenson, C.T.E., and Bennett, N., 2011, The emplacement of the Palaeogene Mourne Granite Centres, Northern Ireland: New results from the Western Mourne Centre: Journal of the Geological Society of London, v. 168, p. 831–836, https://doi.org/10.1144/0016-76492010-123.

Stevenson, C.T.E., Owens, W.H., Hutton, D.H.W., Hood, D.N., and Meighan, I.G., 2007, Laccolithic, as opposed to cauldron subsidence, emplacement of the Eastern Mourne pluton, N. Ireland: Evidence from anisotropy of magnetic susceptibility: Journal of the Geological Society of London, v. 164, p. 99–110, https://doi.org/10.1144/0016076492006-008.

Terzaghi, R.D., 1965, Sources of Error in Joint Surveys: Geotechnique, v. 15, p. 287–304, https://doi.org/10.1680/geot.1965.15.3.287.

Thompson, P., Mussett, A.E., and Dagley, P., 1987, Revised ^{40}Ar-^{39}Ar age for granites of the Mourne Mountains, Ireland: Scottish Journal of Geology, v. 23, p. 215–220, https://doi.org/10.1144/sjg23020215.

Tikoff, B., de Saint Blanquat, M., and Teyssier, C., 1999, Translation and the resolution of the pluton space problem: Journal of Structural Geology, v. 21, p. 1109–1117, https://doi.org/10.1016/S0191-8141(99)00058-9.

Tomkeieff, S.I., and Marshall, C.E., 1935, The Mourne Dyke Swarm: Quarterly Journal of the Geological Society of London, v. 91, p. 251–292, https://doi.org/10.1144/GSL.JGS.1935.091.01-04.10.

Traill, W.A., 1871, Sheet 61, Ardglass, *in* Geological Survey of Ireland 1:63,360 geological map series, Dublin, Ordnance Survey.

van Wyk de Vries, B., Márquez, A., Herrera, R., Bruña, J.L.G., Llanes, P., and Delcamp, A., 2014, Craters of elevation revisited: Forced-folds, bulging and uplift of volcanoes: Bulletin of Volcanology, v. 76, p. 875, https://doi.org/10.1007/s00445-014-0875-x.

Walker, G.P.L., 1975, A new concept of the evolution of the British Tertiary intrusive centres: Journal of the Geological Society of London, v. 131, p. 121–141, https://doi.org/10.1144/gsjgs.131.2.0121.

Wilkinson, C.M., Ganerød, M., Hendriks, B.W.H., and Eide, E.A., 2017, Compilation and appraisal of geochronological data from the North Atlantic Igneous Province (NAIP): Geological Society of London, Special Publications, v. 447, p. 69–103, https://doi.org/10.1144/SP447.10.

Wilson, P.I.R., McCaffrey, K.J.W., Wilson, R.W., Jarvis, I., and Holdsworth, R.E., 2016, Deformation structures associated with the Trachyte Mesa intrusion, Henry Mountains, Utah: Implications for sill and laccolith emplacement mechanisms: Journal of Structural Geology, v. 87, p. 30–46, https://doi.org/10.1016/j.jsg.2016.04.001.

Woodcock, N.H., and Underhill, J.R., 1987, Emplacement-related fault patterns around the Northern Granite, Arran, Scotland: Geological Society of America Bulletin, v. 98, p. 515, https://doi.org/10.1130/0016-7606(1987)98<515:EFPATN>2.0.CO;2.

Yoshinobu, A.S., Fowler, T.K., Paterson, S.R., Llambias, E., Tickyj, H., and Sato, A.M., 2003, A view from the roof: Magmatic stoping in the shallow crust, Chita pluton, Argentina: Journal of Structural Geology, v. 25, p. 1037–1048, https://doi.org/10.1016/S0191-8141(02)00149-9.

Zeeb, C., Gomez-Rivas, E., Bons, P.D., and Blum, P., 2013, Evaluation of sampling methods for fracture network characterization using outcrops: American Association of American Petrologists Bulletin, v. 97, p. 1545–1566, https://doi.org/10.1306/02131312042.